Published in final edited form as:
Langmuir. 2010 June 1; 26(11): . doi:10.1021/la904793t.

Kinetic Assembly of Near-IR Active Gold Nanoclusters using Weakly Adsorbing Polymers to Control Size

Jasmine M. Tam[1], **Avinash K. Murthy**[1], **Davis R. Ingram**[1], **Robin Nguyen**[1], **Konstantin V. Sokolov**[2,3], and **Keith P. Johnston**[1]

[1]Department of Chemical Engineering, The University of Texas at Austin, Austin, TX 78712

[2]Department of Biomedical Engineering, The University of Texas at Austin, Austin, Texas 78712

[3]Department of Biomedical Engineering, M.D. Anderson Cancer Center, Houston, Texas 77030, USA

Abstract

Clusters of metal nanoparticles with an overall size less than 100 nm and high metal loadings for strong optical functionality, are of interest in various fields including microelectronics, sensors, optoelectronics and biomedical imaging and therapeutics. Herein we assemble ~5 nm gold particles into clusters with controlled size, as small as 30 nm and up to 100 nm, which contain only small amounts of polymeric stabilizers. The assembly is kinetically controlled with weakly adsorbing polymers, PLA(2K)-*b*-PEG(10K)-*b*-PLA(2K) or PEG (MW = 3350), by manipulating electrostatic, van der Waals (VDW), steric, and depletion forces. The cluster size and optical properties are tuned as a function of particle volume fractions and polymer/gold ratios to modulate the interparticle interactions. The close spacing between the constituent gold nanoparticles and high gold loadings (80–85% w/w gold) produce a strong absorbance cross section of ~9×10^{-15} m^2 in the NIR at 700 nm. This morphology results from VDW and depletion attractive interactions that exclude the weakly adsorbed polymeric stabilizer from the cluster interior. The generality of this kinetic assembly platform is demonstrated for gold nanoparticles with a range of surface charges from highly negative to neutral, with the two different polymers.

Introduction

Optical and electronic properties of 1D[1], 2D, and 3D clusters of metal nanocrystals, 20 to 500 nm in diameter, have been studied extensively, especially for applications involving sensors, memory devices, microelectronics[2–4], and more recently, for cellular imaging and therapy[5–9]. For a variety of applications, robust and broadly applicable synthetic strategies are needed to pack high levels of functionality (i.e. high metal loadings) into clusters with an overall size smaller than ~30 to 100 nm. Most often, clusters are formed by thermodynamic self assembly. Rotello and co-workers developed a “bricks and mortar” technique for the templated assembly of metal nanoparticles into clusters using polymers, proteins, and DNA[2, 10] and Glotzer et al. and Miles et al.[11] have demonstrated assembly with polymer-tethered nanoparticles[12]. Gold nanoparticles have been assembled in the cores of block copolymer micelles[13–16] and on the surface of micelles[17, 18]. Amphiphilic gold Janus spheres, containing hydrophobic and hydrophilic domains self-assemble into clusters[19–22]

Supporting Information Available

Explanation of calculations of ligand coverage, lysine displacement of citrate ligands, size distribution moments, extinction cross sections, interaction potentials, and theoretical stability ratios. Figures include ligand schematics, nanocluster reproducibility, characterization of nanoclusters composed of citrate-capped nanoparticles, variance of polymer/gold ratio, and variance of starting gold concentration. This information is available free of charge via the Internet at http://pubs.acs.org/.

upon manipulation of pH or solvent quality. For clusters formed thermodynamically, high concentrations of templating agents and strong interactions between these agents and the particles are typically required to drive the self-assembly. Consequently, these agents are usually highly retained in the final cluster and limit the metal loading, typically well below 50% w/w.

An alternative approach is to form clusters of metal nanoparticles by kinetic assembly to achieve extremely high metal loadings by manipulating van der Waals (VDW), electrostatic, and steric interactions. For example, variation of pH or ionic strength of dilute dispersions of citrate-capped gold nanoparticles screens electrostatic repulsion and induces cluster growth[23, 24]. Similarly, lysine-[25–28] and cysteine-[29] capped gold nanoparticles at high loadings aggregate reversibly in response to changes in charge with pH. Gold nanoparticles coated with associating proteins, such as biotin and streptavidin[30], or with complementary DNA strands[31, 32] also form clusters. However, in each of these cases, uncontrolled growth often yields irregularly shaped aggregates greater than several hundred nanometers in diameter. Therefore, a conflict arises in both thermodynamically- and kinetically-controlled assembly between the need for sufficient levels of stabilizers to arrest growth to produce small sub-100 nm clusters, while simultaneously achieving high metal loadings for high functionality.

Metal nanoparticles with high NIR absorbance are of great interest in biomedical imaging and therapy because soft tissues and water are relatively transparent from 650 to 900 nm. The surface plasmon resonance (SPR) of a spherical gold particle exhibits a maximum at 530 nm, but undergoes a red shift to the NIR for particles with a hollow or non-spherical geometry, such as nanoshells[33–35], nanorods[36, 37], and nanocages[38, 39]. These particles are typically 50–100 nm in diameter. NIR absorbance has rarely been achieved for particles smaller than 50 nm, where it becomes challenging to synthesize the types of asymmetric morphologies needed for strong red-shifts[40]. Significant NIR absorbance also has been demonstrated *in vitro* and *in vivo* for the assembly of 40 nm gold spheres, conjugated with antibodies, by receptors in cancer cells into clusters[5, 6, 8, 41]. Small gold clusters that have been formed by equilibrium self assembly methods often contain high concentrations of templating agents, which result in particle separations greater than one particle diameter and thus small red shifts[42, 43].

Nanoparticle components may be assembled into clusters with properties that are challenging to achieve including, sizes below 50 nm[3, 7, 13, 44] strong optical absorbance[7, 44], multifunctionality[7], and/or biodegradability[9, 44]. Recently, there has been great interest in the development of sub-30 nm particles, which penetrate cell membranes and leaky vasculature in cancerous tumors more efficiently than particles >50 nm[45–49]. Furthermore, these small nanoparticles elicit profound changes in biological pathways in targeted cells. Sub-30 nm particles have been reported for gold nanocages[50] and multifunctional nanocluster hybrids containing gold and iron oxide, referred to as nanoroses[7]. Despite their small sizes, both types of nanoparticles absorb strongly in the NIR. The nanorose clusters, composed of nanocomposite primary particles, are formed by kinetic assembly during the reduction of gold precursors onto iron oxide nanoparticles. They exhibit intense magnetic relaxivity as well as NIR absorbance[7]. To further advance the functional properties in nanoclusters, especially biodegradability, we recently introduced a physical, rather than chemical, method for the kinetically controlled colloidal assembly of ~5 nm gold spheres into ~100 nm NIR plasmonic clusters stabilized by PLA(2K)-*b*-PEG(10K)-*b*-PLA(2K). These clusters were shown to biodegrade nearly completely in solution and in macrophage cells back to the original 5 nm primary spheres, which are small enough for renal clearance[9]. This physical, kinetic, colloidal assembly method is general and likely to enable synthesis of many types of clusters over a wide size range.

Herein we assemble kinetically sub-5 nm gold particles into clusters of controlled sizes, as small as 30 nm and up to 100 nm, stabilized by small amounts of a weakly adsorbing polymer, either PLA-*b*-PEG-*b*-PLA or PEG 3350. The physical cluster assembly process, introduced recently in Tam et al.[9], is illustrated in Fig. 1. The gold nanoparticles are nucleated rapidly at high volume fractions in the presence of a weakly adsorbing polymer to form small clusters[9]. The nucleation and growth of the gold clusters is controlled by increasing gold and polymer concentrations simultaneously, either by solvent evaporation or by mixing of a concentrated gold dispersion with a concentrated polymer solution. A mechanism is presented to describe the cluster growth and gold particle spacing in terms of the electrostatic, VDW, steric and depletion forces. The combination of high gold particle volume fractions and exclusion of the weakly adsorbed polymeric stabilizer from the cluster interior towards the exterior surface are utilized to produce low polymer loadings and closely spaced gold particles for strong NIR absorbance. In contrast, high polymer loadings and larger gold particle spacings are typically obtained in equilibrium assembly processes that rely on strong interactions with templating agents, such as micelles[13–18, 51, 52]. Finally, the small amount of polymer on the exterior surface provides sufficient steric stabilization to prevent unregulated cluster growth, in contrast with previous studies without polymer stabilizers[24–29]. Relative to our previous study[9], the size of the clusters is over three fold smaller, and furthermore, a wider range of ligands (to modify particle charge), polymers, and polymer/gold ratios are examined. An advantage of this kinetic assembly approach is its use of readily available polymer stabilizers and simple ligands on the gold surface, such as citrate and lysine, in contrast to templating agents that often require complicated synthetic approaches.

Experimental

Materials

$HAuCl_4 \cdot 3H_2O$ was purchased from MP Biomedicals LLC (Solon, OH) and $Na_3C_3H_5O(COO)_3 \cdot 2\ H_2O$ and $NaBH_4$ were acquired from Fisher Scientific (Fair Lawn, NJ). L(+)-lysine was obtained from Acros Chemicals (Morris Plains, NJ). PEG (MW=3350) was ordered from Union Carbide (Danbury, CT) and PLA(2K)-*b*-PEG(10K)-*b*-PLA(2K) was purchased from Sigma Aldrich (St. Louis, MO).

Nanocluster formation

Gold nanoparticles (3.8-nm) stabilized with citrate ligands were synthesized based on a well known method[53]. Briefly, DI water (100 mL) was heated to 97°C. While stirring, 1 mL of 1% $HAuCl_4 \cdot 3H_2O$, 1 mL of 1% $Na_3C_3H_5O(COO)_3 \cdot 2\ H_2O$, and 1 mL of 0.075% $NaBH_4$ in a 1% $Na_3C_3H_5O(COO)_3 \cdot 2\ H_2O$ solution were added in 1 minute intervals. The solution was stirred for 5 minutes and then removed to an ice bath to cool to room temperature. The gold particles were then centrifuged at 10,000 rpm for 10 minutes at 4°C to remove any large aggregates. Centrifugal filter devices (Ultracel YM-30, Millipore Co.) were used to remove unadsorbed citrate ligands as well as concentrate the gold dispersion to ~3.0 mg Au/mL. Gold concentrations were determined using flame atomic absorption spectroscopy (FAAS).

In most cases, lysine ligands were added to the citrate stabilized gold nanoparticles by adding a 1% lysine in pH 8.4 phosphate buffer (10 mM) solution to 1.2 mL of the colloidal citrate-capped gold solution to yield a final lysine and gold concentration of 0.4 mg/mL and 3.0 mg/mL, respectively. In the cases where a 1.0 mg/mL gold solution was used to produce nanoclusters, the 3.0 mg/mL stock gold solution was diluted using deionized (DI) water. The dispersion was stirred for at least 12 hours[26, 54]. PLA-*b*-PEG-*b*-PLA was added to the aqueous dispersion of ligand capped gold nanoparticles to yield polymer/gold ratios ranging from 1/10 – 40/1. The dispersions were then sonicated in a bath sonicator for 5 minutes.

Unless otherwise noted, the concentration of the gold solutions used in this study to produce nanoclusters was 3.0 mg/mL with a polymer/gold ratio of 16/1.

In some cases, the polymer/gold dispersion was placed under an air stream and a certain percentage of the solvent, between 50–100%, was evaporated. The extent of solvent evaporation was determined volumetrically, by comparing the initial and final volume of the dispersion before and after evaporation, using the height of liquid in the vial as a measure of volume. When the dispersion was not dried to completion, it was quenched with DI water after the chosen amount of solvent evaporation. Upon quenching, the concentration of the dispersion was approximately an order of magnitude lower than that of the original gold stock prior to solvent evaporation. In the case of 100% solvent evaporation, which took place over ~20–30 minutes, the dried film was redispersed with 10 mL of DI water to yield a blue dispersion of ~0.30 mg Au/mL. Nanoclusters were also formed using a mixing procedure, in which highly concentrated solutions of gold colloid and polymer were mixed together using a probe sonicator (Branson Sonifier 450, Branson Ultrasonics Corporation, Danbury, CT) with a 102 converter and tip operated in pulse mode at 35 W.

Nanocluster characterization

Nanocluster morphology was observed by transmission electron (TEM) and scanning electron microscopy (SEM). TEM was performed on a FEI TECNAI G2 F20 X-TWIN TEM using a high-angle annular dark field detector. TEM samples were prepared using a “flash-freezing” technique, in which a 200 mesh carbon-coated copper TEM grid was cooled using liquid nitrogen and then dipped into a dilute aqueous nanocluster dispersion. The TEM grid was dried using a Virtis Advantage Tray Lyophilizer (Virtis Company, Gardiner, NY) with 2 hours of primary drying at −40°C followed by a 12 hour ramp to +25°C and then 2 hours of secondary drying at 25°C. Separation distances between primary particles within the nanoclusters were measured by analyzing TEM images using Scion Image software (Frederick, Maryland). A Zeiss Supra 40VP field emission SEM was operated at an accelerating voltage of 5−10 kV. SEM samples were prepared by depositing a dilute aqueous dispersion of the nanoclusters onto a silicon wafer. The sample was dried in a hood, washed with DI water to remove excess polymer, and dried again. UV−visible spectra were measured using a Varian Cary 5000 spectrophotometer for a 1 cm path length. Dynamic light scattering (DLS) measurements of hydrodynamic diameter and zeta potential measurements were performed in triplicate on a Brookhaven Instruments ZetaPlus dynamic light scattering apparatus at a scattering angle of 90° and temperature of 25 °C[55]. Dispersion concentrations were adjusted with either DI water for DLS measurements or pH=7.4 buffer (10 mM) for zeta potential measurements to give a measured count rate between 300–400 kcps. For DLS measurements, all dispersions were filtered through a 0.2 μm filter and probe sonicated for 2 min prior to measurement. The data were analyzed using a digital autocorrelator (Brookhaven BI-9000AT) with a non-negative least-squares (NNLS) method (Brookhaven 9KDLSW32). A distribution of hydrodynamic diameters was obtained based on the Stokes-Einstein equation for the diffusion coefficient of a sphere. All distributions were weighted by volume. Reported average diameters correspond to the D_{50}, or diameter at which the cumulative sample volume was under 50%. For zeta potential measurements, the average value of at least three data points was reported. Thermogravimetric analysis (TGA) was used to determine the amount of adsorbed ligand mass on the primary gold nanoparticles and the final polymer/gold ratio of the nanoclusters. TGA was performed using a Perkin–Elmer TGA 7 under nitrogen atmosphere at a gas flow rate of 20 mL/min. Excess, unadsorbed organic material, either ligands and/or polymer, was removed from particles, either colloidal gold or nanoclusters, by centrifuging the dispersions at 10,000 rpm for 5 minutes at 4°C. For the colloidal gold particles, which were too small to settle efficiently during centrifugation, centrifugal filter devices were used to separate and filter

the particles from the smaller unadsorbed ligands. The supernatants were discarded and the pellets were dried to a powder. The powder samples were held at 50°C for 120 minutes to remove any moisture in the sample and then heated at a constant rate of 20 °C/min from 50°C to 800 °C and held at 800°C for 30 minutes. The loss in mass after heating accounted for the organic component of the particles. Flame atomic absorption spectroscopy (FAAS) was used to determine the gold concentration in the dispersion and the yield for the gold particles that were incorporated into the clusters. A GBC 908AA flame atomic absorption spectrometer (GBC Scientific Equipment Pty Ltd) was used to determine the amount of gold present in a sample. All measurements were conducted at 242.8 nm using an air-acetylene flame. To determine clustering efficiency, a dispersion of nanoclusters of known concentration was centrifuged at 10,000 rpm for 10 minutes at 4°C. FAAS measurements were conducted on the supernatant.

Determination of stability ratio and half-life for aggregation

The stability of the nanoparticles may be quantified using a stability ratio, *W*, defined as the ratio of the rate of fast, diffusion controlled aggregation to slow, kinetically-controlled aggregation[24, 56]. Alternately, *W* may also be determined using the respective half-lives for fast and slow aggregation.

$$W=\frac{k_f}{k_s}=\frac{t_{1/2,s}}{t_{1/2,f}} \quad (1)$$

where k_f and k_s are the rate constants for fast and slow flocculation, respectively, and $t_{1/2,f}$ and $t_{1/2,s}$ are the half-lives for fast and slow flocculation, respectively. The half life for fast, diffusion-controlled aggregation according to Smoluchowski[24, 56] is given as:

$$t_{1/2,f}=\frac{3\eta}{4k_bTN_0} \quad (2)$$

where η is the solution viscosity, and N_0 is the initial number density of nanoparticles. Slow flocculation half-lives were estimated experimentally based on the observed time required for a visual color change in the nanocluster dispersion to occur, t_{col}. The observed t_{col} may be used to estimate half-lives using the assumption that a color change corresponds to the collision of 11 particles[57] and solving the equation for second order reaction kinetics, $1/N(t) = kt + 1/N_0$, to yield:

$$t_{1/2,s}=t_{col}/10 \quad (3)$$

where *N* is the number of particles in the system at time, *t*, and *k* is the reaction rate constant. A more accurate half-life may be determined for particle conversions in excess of 20% via the numerical solution to the Smoluchowski equation, which utilizes a constant collision frequency factor (reaction kernel). Since the half-life for this approach was within a factor of two of the value for the second order kinetics for these conditions, we did not use this more complex model[58].

Results

Effect of particle volume fraction on nanocluster size and optical properties

The amount of ligands on the surface of the gold particles was determined prior to the formation of nanoclusters. For the citrate-capped gold nanoparticles, the average diameter was 3.8 ± 1.0 nm (data not shown) and the zeta potential was −44.0 ± 4.7 mV (Table 1) at a pH of ~7.2. The citrate coverage on the gold nanoparticles was estimated to be about 6.3%

w/w, based on calculations assuming saturated ligand coverage on the 4 nm gold particle surface in good agreement with the 7% w/w citrate measured by TGA(See supplementary). The adsorption of lysine to gold did not significantly change the particle size, which was 4.1 ± 0.8 nm (Fig. 2a), nor the pH of the gold dispersion. Lysine contains two NH_3^+ charges and one COO^- charge over a pH range from 3 to 10[26] (Fig. S1). The ligand exchange with the positively charged lysine increased the zeta potential to −30.1 ± 2.4 mV (Table 1), indicating about 30% of the adsorbed citrate was exchanged(See supplementary). The citrate/lysine-capped particles were coated with 11% total ligand, according to TGA results, compared with 7% for the citrate-only stabilized nanoparticles. The color did not vary for the citrate-only and citrate/lysine-capped gold nanoparticle dispersions for ~1 month, corresponding to a very high W of ~7×10^9 (Table 2) for an N_0 of ~10^{21} particles/m^3 and $t_{1/2,f}$ of 3.93×10^{-5} s, which is based on a gold loading of 3 mg/mL. The high stability is due to strong repulsive charges on the ligands of the particles, in good agreement with previous reports in literature[26, 59].

To form gold clusters, interactions between citrate/lysine gold particles were mediated with a weakly adsorbing polymer, either PLA-*b*-PEG-*b*-PLA, as shown in Fig. 1, or PEG (MW=3350) homopolymer. Without any solvent evaporation, the addition of either polymer to the ligand-capped gold particles at a 16/1 polymer/gold ratio (gold concentration = 3 mg/mL) did not produce a color change over a period of one hour, indicating that clusters of closely-spaced gold were not formed[9]. After an hour, the color slowly changed. A one hour stability (t_{col}=1 hr) corresponds to a maximum W of ~4×10^5, as determined from Eqs. 1–3 (Table 2). To more fully probe the kinetics of nanocluster formation, the nanocluster size was monitored as a function of solvent evaporation by quenching cluster growth with the addition of DI water after a specified level of solvent evaporation. The harvested nanoclusters were observed by TEM (Fig. 2) and their sizes determined by DLS (Fig. 3a). For PLA-*b*-PEG-*b*-PLA, the formation of dimers and trimers was detected, indicating nucleation, after 50% solvent evaporation (Figs. 2, 3a), which occurred over ~5 minutes for a 1.4 mL sample. This time corresponds to a maximum W of ~2.5×10^5, as $t_{1/2,s}$ could have been even smaller than 5 minutes. These small oligomers produced a shoulder in the DLS size distribution. When the suspension, from which 50% of the solvent had been evaporated, was allowed to sit over the course of one week, still no color change was observed, indicating that the oligomers did not grow to produce larger clusters. However, additional solvent reduction to 60% evaporation, approximately one minute later, led to clusters 35–60 nm in size, as seen both by TEM and DLS. Further solvent evaporation, to 80% and 100%, produced additional growth, with D_{50} values of 60 nm and 80 nm, respectively, with low polydispersities between 1.1–1.8 (See supplementary for calculation). From 50 to 95% evaporation, the cluster size was monotonic with the extent of evaporation. The small, but distinct secondary peaks observed in the particle size distributions for the nanoclusters may indicate coagulation of clusters. These large aggregates composed a very small percentage of the total nanocluster population and were easily filtered out in subsequent experiments. Yields of gold in the clusters, or the percent of the loaded primary particles that are incorporated into clusters after quenching the growth, was determined using FAAS (Table 3). After 60% and 100% solvent evaporation, 95.1% and 99.7%, respectively, of the initially loaded gold nanoparticles by mass were incorporated into clusters. Therefore, cluster yields, as well as size, continued to increase with the extent of solvent evaporation. The ability to tune the cluster size over a wide range and to achieve low polydispersities is of great scientific and practical interest.

Extents of solvent evaporation greater than 60% resulted in a color change of the dispersion to blue, but it was difficult to observe the kinetics given the dark, opaque dispersions at the high volume fractions. Thus, the spectra were measured after the clusters were quenched by dilution. The increase in the NIR absorbance was consistent with the morphologies observed

by TEM and the sizes measured by DLS. Before polymer was added, the characteristic spectrum for individual gold particles exhibited a maximum at 530 nm (Fig. 3b). For the dimers and trimers (Fig. 2b), the red-shift was modest as expected[42, 43, 60]. A much larger increase in the NIR absorbance was observed for 60% evaporation (Fig. 3b), where sizable clusters of 35–60 nm were observed by TEM and DLS, as expected from theoretical calculations[42, 43, 60]. The NIR absorbance continued to increase as the extent of evaporation and nanocluster size increased.

Complete solvent evaporation produced a smooth blue film on the glass surfaces of the vials, indicating a shift in the absorbance spectra of gold to the NIR. Reconstitution of the film with DI water yielded a dark blue dispersion of sub-100 nm clusters composed of primary gold nanoparticles (Fig. 2)[9]. SEM images of nanoclusters formed after 100% solvent evaporation reveal a polymer-rich shell a few nanometers thick surrounding the exterior of each cluster. The spectra of the nanoclusters formed after 100% solvent evaporation exhibited a broad, relatively constant, absorbance in the important NIR region from 700 to 900 nm, corresponding to an extinction coefficient at the maximum absorbance, ε_{703}, of 0.017 $cm^2/\mu g$ for a 56 μg/mL gold dispersion. Assuming that the gold nanoparticles occupy ~72% of the cluster volume (based on SEM and TEM images in Fig. 2), characteristic of a closest-packed volume fraction, the estimated particle extinction cross section was 9.0×10^{-15} m^2 (See supplementary), comparable to the value for nanoshells[42], nanocages[39], nanorods[42], and nanoroses[7]. The mean spacing between primary gold particles within the clusters was estimated to be 1.80 ± 0.6 nm[9], well within the range of interparticle spacing known to produce a significant red-shift in the SPR[1, 42, 43]. The ability of the gold nanoparticles to pack tightly together is supported by TGA results, which indicated that after 100% solvent evaporation, nanoclusters contained only 20 ± 5% organic material. From the known amount of ligand reported above, 10–15% of this material was polymer. The ability to reproducibly produce nanoclusters using 100% evaporation, with respect to both size and optical properties, is shown in Fig. S2. Furthermore, these nanoparticles exhibited excellent stability in terms of particle size and optical properties over the course of 3 weeks, as determined by DLS and UV-vis measurements (data not shown). Nanoclusters were stored in a refrigerator at 4°C between measurements.

The zeta potentials of the resultant nanoclusters of citrate-only and citrate/lysine-capped nanoparticles were −13.0 ± 3.3 mV and −16.3 ± 4.0 mV, respectively, approximately half that of the initial colloidal gold nanoparticles (Table 1). Interestingly, the zeta potential of clusters formed using citrate-only and citrate/lysine-capped gold, stabilized with PLA-*b*-PEG-*b*-PLA, had similar zeta potential values, somewhat larger than that of the pure polymer. The value of −8.0 ± 0.2 mV for the PLA-*b*-PEG-*b*-PLA polymer is attributed to the ionized PLA end groups.

Nanoclusters were also formed using PEG (MW=3350), instead of PLA-*b*-PEG-*b*-PLA, as the stabilizing polymer. The PEG-stabilized clusters were, on average, ~1.5 times larger than those stabilized using PLA-*b*-PEG-*b*-PLA, as reported by DLS and TEM (Fig. 4a–c). Similar to observations for PLA-*b*-PEG-*b*-PLA-stabilized clusters, a reduction in solvent evaporation from 100% to 60% yielded a ~30% reduction in cluster size and slightly lower NIR absorbances. The strong NIR absorbance of the PEG-stabilized clusters indicated that tight packing of gold nanoparticles within the cluster was achieved (Fig. 4d). In fact, the clusters formed at 60% solvent evaporation show a slightly stronger NIR absorbance than the clusters formed after 60% solvent evaporation using PLA-*b*-PEG-*b*-PLA, likely due to the larger cluster size. Similar trends were obtained for nanoclusters produced using citrate-only capped gold nanoparticles and PEG 3350 (data not shown).

Clusters of lysine/citrate particles with PLA-b-PEG-b-PLA formed by mixing

Assembly of nanoclusters was also demonstrated without solvent evaporation by mixing together highly concentrated gold and polymer solutions. The resulting concentrations of gold particles and polymer corresponded to those achieved by certain solvent evaporation extents. For example, a 6 mg/mL dispersion of gold nanoparticles was mixed with a 100 mg/mL polymer solution to produce clusters that were equivalent to the concentrations achieved after 50% evaporation. However, the cluster sizes were at least 2.5 times larger than those where the particle volume fractions were increased gradually by solvent evaporation (Fig. 5a). Furthermore, nanoclusters formed by mixing, instead of solvent evaporation, tended to form a larger amount of aggregates of nanoclusters, as indicated by the more prominent secondary peaks in the particle size distributions. Because of their larger sizes, nanoclusters produced by this method displayed even more shifted NIR absorbance (Fig. 5b). Similar trends in optical properties were observed when clusters of citrate-only-capped gold nanoparticles were produced using this mixing method (Fig. S3). The high viscosities of the extremely concentrated polymer solutions, ranging from 9×10^{-4} Pa s (~10 times that of water) to 0.8 Pa s (~900 times that of water) for solutions corresponding to 60% and 90% solvent evaporation (Fig. S4), respectively, resulted in inadequate mixing rates, poorer polymer diffusion, and thus the larger clusters with an increased propensity to form aggregates.

Clusters formed with citrate-only capped particles and PEG-SH coated particles

Nanoclusters were produced using gold nanoparticles capped with two other types of ligands: negatively charged citrate, and neutral PEG-SH to compliment the above studies which used lysine (positively charged) and citrate ligands, simultaneously. Clusters of gold primary particles capped with either citrate or a citrate/lysine mixture exhibited strong NIR absorbance (Fig. 6). However, nanoparticles capped with PEG-SH did not produce a significant red-shift, although the shift was larger for PEG-SH with a MW of 0.13K versus 5K. PEG-SH 5K has a reported radius of gyration of 3.1 nm[61]. Therefore, the corresponding particle separations between two PEG-SH coated particles of at least 6.2 nm is larger than the diameter of a gold primary particle and the strongly bound PEG-SH 5K ligands prevented the gold nanoparticles from packing together tightly enough for a strong red shift.

Relative to citrate/lysine-capped particles, very similar behavior was observed for clusters assembled with citrate-only capped gold nanoparticles and PLA-*b*-PEG-*b*-PLA upon solvent evaporation, according to DLS, TEM, and UV-vis/NIR measurements (Fig. S5). Again, there was a very strong correlation between cluster size and NIR absorbance. However, the clusters did not form until ~ 85% solvent evaporation, as compared to 60% for citrate/lysine capped gold (Fig. 7). The greater repulsion for the citrate-only-capped particles, as is evident in the larger zeta potentials, appeared to delay cluster formation. The slightly smaller sizes and larger SPR red-shifts of the nanocluster composed of citrate/lysine nanoparticles may be influenced by the attractive electrostatic attraction between the positive and negative charges on the lysine (Fig. S1)[26]. These interactions may further promote polymer exclusion from the cluster interior.

Tuning cluster size with polymer/gold ratio

To demonstrate the ability to tune the cluster size, the gold loading was lowered to 1.0 mg/mL, compared to 3.0 mg/mL in our previous study[9], and the polymer/gold ratio was varied over a wide range for 100% solvent evaporation. Cluster sizes decreased considerably as polymer/gold ratios were reduced from 16/1 to 1/1 (Fig. 8a), with an average diameter of 28.4 nm for the 1/1 ratio. Despite the reduction in cluster size, clusters produced at a polymer/gold ratio between 1/1 to 16/1 still exhibited a broad and intense NIR absorbance, similar to that shown in Fig. 3b. However, for polymer/gold ratios below 1/1, the absorbance

did not shift significantly from that of colloidal gold (Fig. 8b). For a given polymer/gold ratio, similar results were obtained for the cluster size and spectra for the higher gold loading of 3.0 mg/mL, as shown in Fig. S6, although the sizes were slightly smaller for the 1.0 versus the 3.0 mg/mL loading. As an example of the extent by which the cluster sizes could be tuned, the much smaller clusters formed with a 1/1 polymer/gold ratio at a gold loading of 1.0 mg/mL versus a 16/1 polymer/gold ratio at a 3.0 mg/mL loading is shown in TEM micrographs (Fig. 8c–d). Additionally, a small decrease in the absorbance spectra was observed for clusters formed at a 40/1 polymer/gold ratio and a 3.0 mg/mL gold loading (Fig. S6b). Here, an extremely high polymer concentration of 1200 mg/mL was generated when the level of solvent evaporation reached 90%, resulting in excessive polymer that likely interfered with close-spacing between the gold nanoparticles, and thus, lowered the red shift[43]. This interference was not present for lower polymer/gold ratios. Further decreasing gold loadings as low as 0.19 mg/mL and increasing the polymer/gold ratio up to 260/1 led to the formation of increasingly larger clusters with reduced NIR absorbance (Table S1, Fig. S7). Nanoclusters produced at a 1/1 gold/polymer ratio and a 1.0 mg/mL gold concentration were approximately 85% gold w/w, comparable to 80% w/w gold in nanoclusters formed with a 16/1 gold/polymer ratio and a starting gold concentration of 3.0 mg/mL, as determined by TGA.

Discussion

Interaction potential and stability ratio

The kinetic assembly of nanoparticles into clusters may be controlled by adjusting the stability ratio for a pair of particles, which is dependent upon the total interaction potential between particles:

$$V_{total} = V_{electrostatic} + V_{VDW} + V_{steric} + V_{depletion} \quad (4)$$

The first two terms are described by DLVO theory, as discussed in the supplementary section. The addition of a weakly or non-adsorbing polymer introduces attractive depletion interactions, which arise from the exclusion of polymer from the gap region between two particle surfaces. The depletion potential for hard sphere colloids and polymers treated as “penetrable hard spheres” is given by[62–65]:

$$\frac{V_{depletion}(H)}{k_b T} = -\rho_\infty \pi \left[\frac{4}{3}r^3 + 2r^2 a - r^2 H - 2raH + \frac{aH^2}{2} + \frac{H^3}{12}\right], 0 \le H < 2r \quad (5)$$

where H is the distance between particle surfaces, r is the polymer radius, a is the nanoparticle radius, and ρ_∞ is the number density of polymer particles in solution. If the polymer forms micelles, the micellar properties are used (See supplementary). The ability of depletion forces to cause particle flocculation, and even phase separation, in colloid-polymer mixtures is well known both experimentally and theoretically[66–68]. The kinetic stability ratio, in terms of V_{total}, is described by[55]

$$W = 2a \int_{2a}^{\infty} \frac{\frac{D_\infty}{D(u)} \left[\exp\left(\frac{V_{total}}{k_b T}\right)\right]}{H^2} dH \quad (6)$$

where u is a dimensionless variable defined as $(H-2a)/a$, and the ratio $D_\infty/D(u)$ is the hydrodynamic correction factor:

$$\frac{D_\infty}{D(u)} = \frac{6u^2+13u+2}{6u^2+4u} \quad (7)$$

The first parts of the discussion section compare the kinetically controlled nanocluster assembly with previous studies based on the terms for V_{total} and the manipulation of the particle concentrations. A quantitative expression is not presented herein for V_{steric}, given the complexity of hydration of PEG at high concentrations where gels are formed.

Cluster assembly in the absence of polymer (VDW and electrostatic forces)

In the absence of a polymer, the VDW and electrostatic terms play a primary role in cluster formation, whereas steric and depletion interactions are small. Electrostatic repulsion of the nanoparticles may be weakened by a change in pH or salinity to reduce the charge. For dilute dispersions of gold coated with citrate (0.1 mg gold/mL), the growth from attractive VDW forces may be controlled over a period of hours to form clusters >100 nm in size[23, 24]. For these dilute conditions, the clusters are typically relatively low density with a low fractal dimension. In contrast, clusters formed at high particle concentrations are more likely to be composed of gold particles with close spacing that favors strong NIR absorbance. However, for concentrated gold dispersions (20–50 mg/mL), it becomes difficult to balance the electrostatic repulsion and VDW attraction to control the growth, and substantial aggregation has been observed over a period of several minutes[26]. For instance, when gold nanoparticles are capped with lysine ligands, a change in pH simultaneously produces both positive and negative charges (Fig. S1) that result in electrostatic attraction and irregularly shaped aggregates up to several microns in diameter[23, 25–28]. Additional concepts in kinetic assembly are needed to better control V_{total} and thus the particle size and gold spacing

Cluster assembly in the presence of polymer

The key challenge in this study was to control nanocluster size and gold particle spacing within the clusters by manipulation of the particle concentration pathways and V_{total}. High gold particle concentrations (>>0.1 mg/mL) were utilized in order to achieve sufficiently close gold particle spacing for strong NIR absorbance. However, they can also cause unmitigated cluster growth. This dilemma was addressed by the addition of a weakly adsorbing polymer to manipulate the electrostatic, steric, and depletion forces. The polymer initiates nucleation and growth, while simultaneously providing steric stabilization, but with low final polymer loadings.[2, 18, 51]

The initial citrate-only and citrate/lysine-capped gold nanoparticles in this study were extremely stable, evidenced by large negative zeta potentials of −44 and −30 mV, respectively, and a V_{total} of at least 23 k_BT (Fig. 9) (See supplementary). Nanocluster formation was initiated by raising the polymer and gold particle concentrations either by solvent evaporation or mixing to raise the adsorption of the polymer on gold. The weakly adsorbed polymer decreases the local dielectric constant near the charged ligands and thus weakens the ion hydration, causing ion pairing. This decrease in particle charge is directly evident in the decrease in the zeta potential with the addition of polymer (Table 1). The decrease in electrostatic repulsion causes a marked decrease in the experimentally determined W (Table 2) from ~10^{10} for the citrate/lysine-capped primary particles to ~10^5 after the addition of polymer and 50% solvent evaporation. At this condition, the polymer adsorption did not reduce the particle charge enough to produce clusters larger than dimers or trimers within several hours.

At an extent of 50% solvent evaporation, the charge on an individual gold particle was regressed from the theoretical W in Eq. 6, given the known experimental W described above

(Table 2). In this regression, V_{total} included electrostatic, VDW, and depletions terms, as described in the supplementary section. V_{steric} was not included in the regression because its role during the aggregation process was assumed to be relatively small, given the much larger magnitude of the electrostatic repulsion for the weakly adsorbed polymer. However, the role of steric stabilization for the fully-formed nanoclusters is more significant, as the polymer is excluded towards the outside of the clusters. All of the properties were known except the surface potential (and thus surface charge) on a gold nanoparticle. The reduction in the regressed surface charge of 1.6 after 50% solvent evaporation, relative to that of the initial colloidal gold particles, was found to be comparable to the reduction in zeta potential given in Table 1. The loss in charge is further characterized by the large decrease in V_{total} to about 11 k_BT (Fig. 9), which may be attributed to the significant drop in $V_{electrostatic}$ upon charge reduction caused by the polymer, as V_{VDW} did not change. Thus, this large decrease in $V_{electrostatic}$, and consequently V_{total}, produced a decrease in W at 50% solvent evaporation of 5 orders of magnitude, relative to the initial colloidal gold particles (Fig. 10). It was not possible to regress any changes in the particle charge with higher extents of solvent evaporation because the dispersions were too turbid to determine W experimentally. The regressed charge at 50% was used to calculate the V_{total} and thus W for greater solvent evaporation levels. V_{total} decreased as solvent evaporation increased, primarily due to a reduction in $V_{electrostatic}$. Using Eq. 6, the steady decrease in $V_{electrostatic}$, and thus V_{total}, with solvent evaporation (i.e. increasing particle volume fraction) was found to cause a further decrease in W (Fig. 10). The $V_{electrostatic}$ decreases with an increase in the number density of charged gold nanoparticles as the extent of evaporation increases. For electro-neutrality, the resulting increase in counter-ion concentration reduces the Debye length according to Eq. S12. However this change in $V_{electrostatic}$ changes W by less than an order of magnitude, significantly smaller than the changes observed with polymer induced ion pairing. Therefore, the initial cluster growth is driven primarily by the attractive VDW forces upon reduction of particle charge and electrostatic repulsion upon weak polymer adsorption[66, 69]. As the number of closely-spaced gold particles in the cluster increases, the number of water molecules in the coordination shells about each particle decreases, given that the gold surface is hydrophobic. This decrease in hydration may further contribute to ion pairing and weakened electrostatic repulsion.

The smaller clusters produced using PLA-*b*-PEG-*b*-PLA as a stabilizer versus PEG homopolymer may be attributed to the stronger adsorption of the more hydrophobic PLA-*b*-PEG-*b*-PLA[16, 70], which produces greater charge reduction and thus more rapid nucleation. The larger number of nuclei and greater steric stabilization for reduced growth would lead to small clusters. Furthermore, the presence of micelles for PLA-*b*-PEG-*b*-PLA may provide greater steric stabilization than the homopolymer in the early stages of growth. Similarly, smaller clusters formed for the less charged citrate/lysine-capped gold versus citrate-only capped gold (Fig. 7) may also be attributed to more rapid nucleation. In addition, the attractive electrostatic interactions between the lysine ligands may enhance polymer exclusion from the cluster interior.

The decrease in $V_{electrostatic}$ to drive cluster growth may also be achieved simply by adding salts. However, without the steric and depletion contributions to the potential, control over the final cluster size for high initial gold particle concentrations has not been successful[23, 24]. Thus, manipulation of these additional terms with polymer concentration and structure is important to achieve greater control over kinetic self-assembly. The nucleation of clusters via an adsorbed polymer to reduce the surface charge and simultaneously provide steric stabilization enables significantly improved control over cluster growth even with the high gold particle concentrations.

Spacing between gold particles in the nanoclusters

The final polymer weight fraction in the clusters was only on the order of 10 to 15% w/w according to TGA, even with starting polymer/gold ratios well above unity, for example our most common case of 16/1. The small spacing between the gold particles of only 1.80 nm[9] for PLA-*b*-PEG-*b*-PLA stabilized nanoclusters is considerably smaller than the size of a PLA-*b*-PEG-*b*-PLA polymer micelle, measured to be 10–14 nm (Fig. S8) or the R_g of the PEG homopolymer of 6.1 nm[71]. Thus, the polymers were excluded from the cluster interior. Various properties of gold contribute to the low polymer loadings, which favor small interparticle distances. The Hamaker constant is 60 k_BT for Au versus only 0.6 k_BT for the PEG, calculated using Lifshitz theory[12]. The gold surface is not highly hydrophilic given that polypropylene oxide adsorbs more strongly to gold than PEG[70]. Thus, the gold particles are strongly attracted to each other by VDW and hydrophobic forces. Additionally, the polymer chains are depleted from the overlap regions in the interior of the clusters towards the cluster exterior in order to raise their conformation entropy, as described by Eq. 5. These depletion forces, along with the propensity for hydrophilic PEG segments to orient towards the aqueous exterior, drive the weakly adsorbed and hence highly mobile polymer away from the cluster interior and towards the exterior cluster interface with water and into bulk water. This mechanism is supported by the polymer shell observed in the SEM image (Fig. 2f), as well as the low polymer loadings. Thus, the hydrophilic PEG segments of the polymer, which are oriented preferentially towards the exterior cluster interface, extend into the aqueous environment and provide steric stabilization. In essence, the close spacing of the gold particles is driven by the strong VDW attraction between the gold particles and the depletion forces which exclude the polymer.

In the case where a strongly adsorbing polymer is used to regulate cluster formation and growth, the polymer is often retained at significantly higher levels within the final cluster than in the present study. Prud'homme et al. have developed a "flash nanoprecipitation" method to mix an organic dispersion of gold and an aqueous phase containing a polymeric stabilizer. The process resulted in relatively high 35% w/w particle loadings in clusters by inducing high supersaturation with rapid "micro-mixing" to kinetically control nucleation and growth[51, 52]. The polymer adsorption was sufficiently strong to passivate the surface of nucleating particles under high supersaturation conditions to produce clusters as small as 80 nm[51]. However, the resultant clusters did not exhibit a shift into the NIR. It is possible that the interactions between the polymer and the gold were too strong to achieve close-packing between the gold particles. In addition, the organic phase may have attracted too much polymer to the gold.

Condensation versus coagulation

Size distribution moments calculated from DLS results (Fig. 3a) suggest that the nanoclusters were formed more by condensation than by coagulation, yet some coagulation was present (See supplementary, Table 3). A high yield of 95% of gold in the cluster was observed after only 60% solvent evaporation. Here, exhaustion of primary particles slows down nanocluster growth by condensation. The substantial growth in cluster size from 60% to 100% solvent evaporation cannot be caused by the remaining 5% gold, since the mass of the clusters is proportional to the diameter cubed. Thus, coagulation was the primary cause of growth at this stage. Close inspection of the TEM images in Fig. 2 shows that the larger nanoclusters, formed after larger extents of evaporation (i.e. greater than 60%), are more irregular in shape relative to a spherical geometry. In fact, one may even discern that the larger clusters are partially composed of smaller, 35–60 nm, clusters, indicating a small degree of coagulation. By quenching the nanocluster dispersion with DI water soon after cluster formation, after only 60% solvent evaporation, the potential for additional coagulation was reduced, thus preserving smaller nanocluster sizes and low polydispersities.

Tuning cluster size with polymer/gold ratio

A reduction in the polymer/gold ratio from 16/1 to 1/1 resulted in a marked decrease in cluster size from ~80 nm to ~30 nm (Fig. 8), as well as a reduction in polymer loading from 20 to 15%, as shown by TGA. This decrease is the opposite of what is expected for steric stabilization alone, indicating other factors were operative. For lower initial polymer/gold ratios and thus polymer concentrations, the lower adsorption onto gold produces a smaller degree of ion pairing and thus a larger $V_{electrostatic}$. The greater repulsion will favor slower growth as observed. Furthermore, the lower polymer concentration reduces the collision frequency between polymer chains and gold clusters, leading to less trapping of polymer in the clusters. Rheological factors are also present. The viscosity of PLA-*b*-PEG-*b*-PLA solutions increases markedly with concentration in the dilute to semi-dilute transition (Fig. S4). During gold cluster formation via solvent evaporation, the viscosity of the dispersion will increase sooner for higher polymer/gold ratios, increasing the amount of entangled polymer that may get trapped within the gold clusters. This behavior was observed as the polymer/gold ratio was raised from 1/1 to 16/1, and was even more prevalent for the 40/1 polymer/gold ratio (Fig. S6). Coagulation was particularly evident at this highest ratio, according to size distribution moment calculations (μ_1=1.55, μ_3=0.81). To examine the effect of polymer gelation, a 50 mg/mL solution of PLA-*b*-PEG-*b*-PLA without gold particles was dried by solvent evaporation. The precipitate was redispersed to give large aggregates (> 500 nm) that did not break up into block copolymer micelles, indicating that gelation was not fully reversible (Fig. S8). For the formation of gold clusters, the gelation of the polymer may make the polymer less available for steric stabilization. Finally, the depletion attraction forces mediate cluster growth both during condensation and coagulation. For smaller polymer/gold ratios, the depletion attraction will decrease, which would favor smaller clusters, as observed (Fig. 8a). As the volume of the gap region increases between particles, the depletion attraction also increases. Thus, the depletion attraction will be larger for two 20 nm, growing clusters than for two primary colloidal 5 nm gold particles. Thus depletion attraction may play a larger role in the later coagulation stage than for the initial growth of the smallest embryos.

Comparison to thermodynamic self assembly methods

The mechanism by which our nanoclusters are formed is fundamentally different from equilibrium-based processes, in which particles are assembled into the cores of micelles or at the interface between the core and the corona. In the case of thermodynamic self-assembly, the polymer-gold interactions are inherently stronger and play a much more dominant role, leading to higher polymer loadings and larger gold spacings. The loadings into micelles are governed by entropic and enthalpic interactions between the solute and the micelle core, as well as the interfacial free energy between the core and corona of a micelle[72]. This interfacial free energy increases as the micelle size decreases, due to larger Laplace pressures, especially for micelles smaller than 200 nm[72]. The loadings of small molecules such as pharmaceuticals in the cores of micelles are often less than 25% by weight[72] and typically less than 10%. The loading of a gold particle in a micelle will be even lower because the entropic interactions will be less favorable, given the high molecular weight of the particle. For example, loadings of only < 2% w/w of ~2.4 nm gold particles in ~20 nm polymer micelles has been observed using small angle x-ray scattering (SAXS)[73]. Thus, thermodynamic assembly methods are not likely to incorporate sufficient gold loadings to yield a strong red-shift in the SPR for clusters, especially for sizes smaller than 50 nm. The kinetic nanocluster assembly method in the present study is not restricted by the thermodynamic constraints of micelle encapsulation. The strong van der Waals interactions between the gold particles were the primary driving force for cluster growth, in the presence of the weakly adsorbing polymer. Furthermore, depletion effects promote exclusion of the

polymer to the cluster surface. These interactions lead to much higher loadings than for thermodynamic assembly of gold particles with micelles.

Application to biomedical imaging and therapeutics

Gold nanoparticles with intense NIR absorbance, including nanoshells[33–35], nanorods[36, 37], and nanocages[38, 39], have received extensive attention as biomedical imaging and therapeutic agents. However, while these particles are within the optimal size range of 6–100 nm to exhibit sufficiently long blood residence times for accumulation at disease sites, they are above the threshold size of 5.5 nm required for efficient clearance by the kidneys[74–76]. Furthermore, the metallic bonds between the gold atoms in these particles do not biodegrade. In contrast, our gold nanoclusters, using PLA-b-PEG-b-PLA as the stabilizer, were shown to biodegrade nearly completely in solution and in macrophage cells back to the original 5 nm gold spheres[9]. The ability to further tune the size to 30 nm and to vary composition, as demonstrated in the current study, broadens the scope of biodegradable nanoclusters significantly.

Conclusions

A general kinetic self-assembly method has been introduced to tune the size of hybrid polymer/gold nanoclusters, as small as 30 nm, with closely-spaced gold particles along with unusually low polymer loadings. These properties are achieved by the combination of high initial gold particle volume fractions and the depletion of the weakly adsorbed polymeric stabilizer from the cluster interior. Either evaporation or mixing may be utilized to produce high initial gold particle and polymer concentrations simultaneously to manipulate growth. Here, the polymer adsorbs weakly on the gold and thereby reduces the electrostatic repulsion to nucleate cluster growth. The growth is arrested by small amounts of polymer on the exterior cluster surface, as characterized by SEM and TGA, which provide steric stabilization and minimize coagulation. The closely-spaced particles provide intense NIR absorbance even in clusters as small as 30 nm, a size which is of great interest for manipulation of biological pathways and signaling at the cellular level[77]. This kinetic assembly platform may be used to tune the size, morphology, and optical properties of a widespread variety of clusters with high metal loadings, simply by varying the particle concentration pathways to adjust the colloidal forces. Additionally, the method has been generalized for initial gold particles with varying surface charge. In contrast, higher polymer loadings along with more widely spaced metal particles are often obtained in nanoclusters formed by thermodynamic self-assembly, which requires stronger metal particle-polymer interactions. Kinetically-controlled nanocluster assembly using physical methods offers broad opportunities for the design of nanoclusters for sensors, optoelectronics and biomedical applications, including multi-modal imaging/therapeutic systems, cell-specific targeting, and biodegradable clusters for rapid clearance from the body.

Supplementary Material

Refer to Web version on PubMed Central for supplementary material.

Acknowledgments

This work is supported in part by the STC Program of the National Science Foundation under Agreement No. CHE-9876674, NIH (CA 103830), NIH RO1 EB008821-01, NIH Training Grant # HL07446 and the Welch Foundation (F-1319).

References

1. DeVries GA, Brunnbauer M, Hu Y, Jackson AM, Long B, Neltner BT, Uzun O, Wunsch BH, Stellacci F. Divalent Metal Nanoparticles. Science. 2007; 315(5810):358–361. [PubMed: 17234943]
2. Ofir Y, Samanta B, Rotello VM. Polymer and biopolymer mediated self-assembly of gold nanoparticles. Chemical Soceity Reviews. 2008; 37(9):1814–1825.
3. Boal AK, Ilhan F, DeRouchey JE, Thurn-Albrecht T, Russell TP, Rotello VM. Self-assembly of nanoparticles into structured spherical and network aggregates. Nature. 2000; 404(6779):746–748. [PubMed: 10783884]
4. Ditsch A, Laibinis PE, Wang DIC, Hatton TA. Controlled Clustering and Enhanced Stability of Polymer-Coated Magnetic Nanoparticles. Langmuir. 2005; 21(13):6006–6018. [PubMed: 15952854]
5. Aaron J, Nitin N, Travis K, Kumar S, Collier T, Park SY, Jose-Yacaman M, Coghlan L, Follen M, Richards-Kortum R, Sokolov K. Plasmon resonance coupling of metal nanoparticles for molecular imaging of carcinogenesis in vivo. Journal of Biomedical Optics. 2007; 12(3):034007/1–034007/11. [PubMed: 17614715]
6. Larson TA, Bankson J, Aaron J, Sokolov K. Hybrid plasmonic magnetic nanoparticles as molecular specific agents for MRI/optical imaging and photothermal therapy of cancer cells. Nanotechnology. 2007; 18(32):325101/1–325101/8.
7. Ma, LL.; Feldman, MD.; Tam, JM.; Paranjape, AS.; Cheruku, KK.; Larson, TA.; Tam, JO.; Ingram, DR.; Paramita, V.; Villard, JW.; Clarke, GD.; Jenkins, JT.; Asmis, R.; Sokolov, K.; Chandrasekar, B.; Milner, TE.; Johnston, KP. ACS Nano. ASAP; 2009. Small multifunctional nanoclusters (Nanoroses) for targeted cellular imaging and therapy.
8. Sokolov KV, Follen M, Aaron J, Pavlova I, Malpica A, Lotan R, Richards-Kortum R. Real-time vital optical imaging of precancer using anti-epidermal growth factor receptor antibodies conjugated to gold nanoparticles. Cancer Research. 2003; 63:1999–2004. [PubMed: 12727808]
9. Tam JM, Tam JO, Murthy AK, Ingram DR, Ma LL, Travis KA, Sokolov KV, Johnston KP. Controlled Assembly of Biodegradable Plasmonic Nanoclusters for Near-Infrared Imaging and Therapeutic Applications. **Submitted**.
10. Srivastava S, Samanta B, Arumugam P, Han G, Rotello VM. DNA-mediated assembly of iron platinum (FePt) nanoparticles. Journal of Materials Chemistry. 2007; 17(1):52–55.
11. Miles WCGJD, Huffstetler PP, Reinhold CM, Pothayee N, Caba BL, Boyd JS, Davis RM, Riffle JS. Synthesis and Colloidal Properties of Polyether-Magnetite Complexes in Water and Phosphate-Buffered Saline. Langmuir. 2009; 25:803–813. [PubMed: 19105718]
12. Iacovella CR, Horsch MA, Glotzer SC. Local ordering of polymer-tethered nanospheres and nanorods and the stabilization of the double gyroid phase. The Journal of Chemical Physics. 2008; 129:044902-1–0440902-10. [PubMed: 18681673]
13. Frankamp BL, Uzun O, Ilhan F, Boal AK, Rotello VM. Recognition-Mediated Assembly of Nanoparticles into Micellar Structures with Diblock Copolymers. Journal of the American Chemical Society. 2002; 124(6):892–893. [PubMed: 11829582]
14. Gopidas KR, Whitesell JK, Fox MA. Nanoparticle-Cored Dendrimers: Synthesis and Characterization. Journal of the American Chemical Society. 2003; 125:6491–6502. [PubMed: 12785790]
15. Uzun O, Frankamp BL, Sanyal A, Rotello VM. Recognition-Mediated Assembly of Nanoparticle-Diblock Copolymer Micelles with Controlled Size. Chemistry of Materials. 2006; 18(23):5404–5409.
16. Sakai T, Alexandridis P. Metal nanoparticle synthesis and organization in 1D, 2D and 3D structures formed by amphiphilic block copolymers. PMSE Preprints. 2005; 93:798–799.
17. Li J, He W-D, Sun X-L. Preparation of poly(styrene-b-N-isopropylacrylamide) micelles surface-linked with gold nanoparticles and thermo-responsive ultraviolet-visible absorbance. Journal of Polymer Science, Part A: Polymer Chemistry. 2007; 45(22):5156–5163.

18. Bae KH, Choi SH, Park SY, Lee Y, Park TG. Thermosensitive Pluronic Micelles Stabilized by Shell Cross-Linking with Gold Nanoparticles. Langmuir. 2006; 22(14):6380–6384. [PubMed: 16800702]
19. Isojima T, Suh SK, Vander Sande JB, Hatton TA. Controlled Assembly of Nanoparticle Structures: Spherical and Toroidal Superlattices and Nanoparticle-Coated Polymeric Beads. Langmuir. 2009; 25(14):8292–8298. [PubMed: 19435297]
20. Harada T, Hatton TA. Formation of Highly Ordered Rectangular Nanoparticle Superlattices by the Cooperative Self-Assembly of Nanoparticles and Fatty Molecules. Langmuir. 2009; 25(11):6407–6412. [PubMed: 19466789]
21. Isojima T, Lattuada M, Vander Sande JB, Hatton TA. Reversible Clustering of pH- and Temperature-Responsive Janus Magnetic Nanoparticles. ACS Nano. 2008; 2(9):1799–1806. [PubMed: 19206418]
22. Lattuada M, Hatton TA. Preparation and Controlled Self-Assembly of Janus Magnetic Nanoparticles. Journal of the American Chemical Society. 2007; 129(42):12878–12889. [PubMed: 17910450]
23. Wilcoxon JP, Martin JE, Schaefer DW. Aggregation in colloidal gold. Physical Review A: Atomic, Molecular, and Optical Physics. 1989; 39(5):2675–2688.
24. Chow MK, Zukoski CF. Gold sol formation mechanisms: role of colloidal stability. Journal of Colloid and Interface Science. 1994; 165(1):97–109.
25. Guo Y, Ma Y, Xu L, Li J, Yang W. Conformational Change Induced Reversible Assembly/Disassembly of Poly-L-lysine-Functionalized Gold Nanoparticles. Journal of Physical Chemistry C. 2007; 111(26):9172–9176.
26. Horovitz O, Mocanu A, Tomoaia G, Bobos L, Dubert D, Daian I, Yusanis T, Tomoaia-Cotisel M. Lysine mediated assembly of gold nanoparticles. Studia Universitatis Babes-Bolyai, Chemia. 2007; 52(1):97–108.
27. Murthy VS, Cha JN, Stucky GD, Wong MS. Charge-Driven Flocculation of Poly(L-lysine)-Gold Nanoparticle Assemblies Leading to Hollow Microspheres. Journal of the American Chemical Society. 2004; 126(16):5292–5299. [PubMed: 15099114]
28. Xu L, Guo Y, Xie R, Zhuang J, Yang W, Li T. Three-dimensional assembly of Au nanoparticles using dipeptides. Nanotechnology. 2002; 13(6):725–728.
29. Lim IIS, Ip W, Crew E, Njoki PN, Mott D, Zhong C-J, Pan Y, Zhou S. Homocysteine-mediated reactivity and assembly of gold nanoparticles. Langmuir. 2007; 23(2):826–833. [PubMed: 17209640]
30. Aslan K, Luhrs CC, Perez-Luna VH. Controlled and Reversible Aggregation of Biotinylated Gold Nanoparticles with Streptavidin. Journal of Physical Chemistry B. 2004; 108(40):15631–15639.
31. Lazarides AA, Schatz GC. DNA-Linked Metal Nanosphere Materials: Structural Basis for the Optical Properties. Journal of Physical Chemistry B. 2000; 104(3):460–467.
32. Mirkin CA, Letsinger RL, Mucic RC, Storhoff JJ. A DNA-based method for rationally assembling nanoparticles into macroscopic materials. Nature (London). 1996; 382(6592):607–609. [PubMed: 8757129]
33. Adler DC, Huang S-W, Huber R, Fujimoto JG. Photothermal detection of gold nanoparticles using phase-sensitive optical coherence tomography. Optics Express. 2008; 16(7):4376–4393. [PubMed: 18542535]
34. Hirsch LR, Stafford RJ, Bankson JA, Sershen SR, Rivera B, Price RE, Hazle JD, Halas NJ, West JL. Nanoshell-mediated near-infrared thermal therapy of tumors under magnetic resonance guidance. Proceedings of the National Academy of Sciences of the United States of America. 2003; 100(23):13549–13554. [PubMed: 14597719]
35. Loo C, Lowery A, Halas N, West J, Drezek R. Immunotargeted Nanoshells for Integrated Cancer Imaging and Therapy. Nano Letters. 2005; 5(4):709–711. [PubMed: 15826113]
36. Huang X, El-Sayed IH, Qian W, El-Sayed MA. Cancer Cell Imaging and Photothermal Therapy in the Near-Infrared Region by Using Gold Nanorods. Journal of the American Chemical Society. 2006; 128(6):2115–2120. [PubMed: 16464114]

37. Pissuwan D, Valenzuela SM, Killingsworth MC, Xu X, Cortie MB. Targeted destruction of murine macrophage cells with bioconjugated gold nanorods. Journal of Nanoparticle Research. 2007; 9(6):1109–1124.
38. Chen J, Saeki F, Wiley BJ, Cang H, Cobb MJ, Li Z-Y, Au L, Zhang H, Kimmey MB, Li X, Xia Y. Gold Nanocages: Bioconjugation and Their Potential Use as Optical Imaging Contrast Agents. Nano Letters. 2005; 5(3):473–477. [PubMed: 15755097]
39. Skrabalak SE, Chen J, Au L, Lu X, Li X, Xia Y. Gold nanocages for biomedical applications. Advanced Materials. 2007; 19(20):3177–3184. [PubMed: 18648528]
40. Kreibig, U.; Vollmer, M. Optical Properties of Metal Clusters. Vol. Vol. 25. Berlin, Germany: Springer; 1995.
41. Kumar S, Harrison N, Richards-Kortum R, Sokolov K. Plasmonic Nanosensors for Imaging Intracellular Biomarkers in Live Cells. Nano Letters. 2007; 7(5):1338–1343. [PubMed: 17439187]
42. Jain PK, Lee KS, El-Sayed IH, El-Sayed MA. Calculated Absorption and Scattering Properties of Gold Nanoparticles of Different Size, Shape, and Composition: Applications in Biological Imaging and Biomedicine. Journal of Physical Chemistry B. 2006; 110(14):7238–7248.
43. Khlebtsov B, Zharov V, Melnikov A, Tuchin V, Khlebtsov N. Optical amplification of photothermal therapy with gold nanoparticles and nanoclusters. Nanotechnology. 2006; 17(20): 5167–5179.
44. Troutman TS, Barton JK, Romanowski M. Biodegradable plasmon resonant nanoshells. Advanced Materials. 2008; 20(13):2604–2608. [PubMed: 21494416]
45. Ferrari M. Cancer nanotechnology: opportunities and challenges. Nature Reviews Cancer. 2005; 5(3):161–171.
46. Zhou Y, Jiang K, Chen Y, Liu S. Gold nanoparticle-incorporated core and shell crosslinked micelles fabricated from thermoresponsive block copolymer of N-isopropylacrylamide and a novel primary-amine containing monomer. Journal of Polymer Science, Part A: Polymer Chemistry. 2008; 46(19):6518–6531.
47. Reddy STSMA, Hubbell JA. Targeting dendritic cells with biomaterials: developing the next generation of vaccines. Trends in Immunology. 2006; 27(12):573–579. [PubMed: 17049307]
48. Wang AZBV, Vasilliou CCGUF, Alexis F, Zhang L, Shaikh M, Yuet K, Cima MJ, Langer R, Kantoff PW, Bander NH, Jon S, Farokhzad OC. Superparamagnetic iron oxide nanopartilc-aptamer bioconjugates for combined prostate cancer imaging and therapy. ChemMedChem. 2008; 3(9):1311–1315. [PubMed: 18613203]
49. Weissleder R. Molecular Imaging in Cancer. Science. 2006; 312(5777):1168–1171. [PubMed: 16728630]
50. Xia, Y. Gold nanocages: A new class of plasmonic nanostructures for biomedical applications; ACS National Meeting; August 19–23, 2007; Boston, MA, United States. 2007. p. COLL-528Boston, MA, United States, 2007
51. Gindy ME, Panagiotopoulos AZ, Prud'homme RK. Composite Block Copolymer Stabilized Nanoparticles: Simultaneous Encapsulation of Organic Actives and Inorganic Nanostructures. Langmuir. 2008; 24(1):83–90. [PubMed: 18044945]
52. Gindy ME, Prud'homme RK, Ji S, Hoye TR, Macosko CW. Functional block copolymer nanoparticles for targeted drug delivery and imaging. PMSE Preprints. 2006; 95:989–990.
53. Grabar KC, Allison KJ, Baker BE, Bright RM, Brown KR, Freeman RG, Fox AP, Keating CD, Musick MD, Natan MJ. Two-dimensional arrays of colloidal gold particles: a flexible approach to macroscopic metal surfaces. Langmuir. 1996; 12:23535–2361.
54. Selvakannan PR, Mandal S, Phadtare S, Pasricha R, Sastry M. Capping of Gold Nanoparticles by the Amino Acid Lysine Renders Them Water-Dispersible. Langmuir. 2003; 19(8):3545–3549.
55. Ryoo W, Webber SE, Johnston KP. Water-in-Carbon Dioxide Microemulsions with Methylated Branched Hydrocarbon Surfactants. Industrial & Engineering Chemistry Research. 2003; 42(25): 6348–6358.
56. Hiemenz PC, Rajagopalan R. Principles of Colloid and Surface Chemistry, Third Edition, Revised and Expanded. 1997:688.
57. Kim T, Lee C-H, Joo S-W, Lee K. Kinetics of gold nanoparticle aggregation: Experiments and modeling. Journal of Colloid and Interface Science. 2008; 318(2):238–243. [PubMed: 18022182]

58. Axford, SDT. Theoretical Calculations on Smoluchowski Kinetics: Perikinetic Reactions in Highly Aggregated Systems. London: The Royal Society; 1996. p. 2355-2368.Proceedings: Mathematical, Physical, and Engineering Sciences, London, 1996
59. Brewer SH, Glomm WR, Johnson MC, Knag MK, Franzen S. Probing BSA Binding to Citrate-Coated Gold Nanoparticles and Surfaces. Langmuir. 2005; 21:9303–9307. [PubMed: 16171365]
60. Blatchford CG, Campbell JR, Creighton JA. Plasma Resonance-Enhanced Raman Scattering by Adsorbates on Gold Colloids: The Effects of Aggregation. Surface Science. 1982; 120:445–455.
61. Riley T, Stolnik S, Heald CR, Xiong CD, Garnett MC, Illum L, Davis SS. Physicochemical Evaluation of Nanoparticles Assembled from Poly(lactic acid)-Poly(ethylene glycol) (PLA-PEG) Block Copolymers as Drug Delivery Vehicles. Langmuir. 2001; 17:3168–3174.
62. Kleshchanok D, Tuinier R, Lang PR. Direct measurements of polymer-induced forces. Journal of Physics: Condensed Matter. 2008; 20(7):073101/1–073101/25.
63. Mondain-Monval O, Leal-Calderon F, Phillip J, Bibette J. Depletion Forces in the Presence of Electrostatic Double Layer Repulsion. Physical Review Letters. 1995; 75:3364–3367. [PubMed: 10059565]
64. Vrij A. Polymers at Interfaces and the Interactions in Colloidal Dispersions. Pure and Applied Chemistry. 1976; 48:471–483.
65. Jodar-Reyes AB, Martin-Rodriguez A, Ortega-Vinuesa JL. Effect of the ionic surfactant concentration on the stabilization/destabilization of polystyrene colloidal particles. J. Colloid Interface Sci. FIELD Full Journal Title: Journal of Colloid and Interface Science. 2006; 298(1): 248–257.
66. Gögelein C, Nägele G, Buitenhuis J, Tuinier R, Dhont1 JKG. Polymer depletion-driven cluster aggregation and initial phase separation in charged nanosized colloids. The Journal of Chemical Physics. 2009; 130(20):204905-1–204905-15. [PubMed: 19485479]
67. Mutch KJ, Duijneveldt JSv, Eastoe J. Colloid–polymer mixtures in the protein limit. Soft Matter. 2007; 3:155–167.
68. Mutch KJ, Duijneveldt JSv, Eastoe J, Grillo I, Heenan RK. Small-Angle Neutron Scattering Study of Microemulsion Polymer Mixtures in the Protein Limit. Langmuir. 2008; 24:3053–3060. [PubMed: 18275227]
69. Kline SR, Kaler EW. Aggregation of Colloidal Silica by n-Alkyl Sulfates. Langmuir. 1996; 12:2402–2407.
70. Sakai T, Alexandridis P. Mechanism of Gold Metal Ion Reduction, Nanoparticle Growth and Size Control in Aqueous Amphiphilic Block Copolymer Solutions at Ambient Conditions. Journal of Physical Chemistry B. 2005; 109(16):7766–7777.
71. Agrawal SK, Sanabria-DeLong N, Tew GN, Bhatia SR. Structural Characterization of PLA-PEO-PLA Solutions and Hydrogels: Crystalline vss Amorphous PLA Domains. Macromolecules. 2008; 41:1774–1784.
72. Varun K, Robert KPh. Thermodynamic limits on drug loading in nanoparticle cores. Journal of Pharmaceutical Sciences. 2008; 97(11):4904–4914. [PubMed: 18300278]
73. Huang C-M, Wei K-H, Jeng US, Liang KS. Structural Evolution of Poly(styrene-b-4-vinylpyridine) Diblock Copolymer/Gold Nanoparticle Mixtures from Solution to Solid State. Macromolecules. 2007; 40(14):5067–5074.
74. Betancourt T, Brown B, Brannon-Peppas L. Doxorubicin-loaded PLGA nanoparticles by nanoprecipitation: preparation, characterization and *in vitro* evaluation. Nanomedicine. 2007; 2(2): 220–232.
75. Kooi MECVC, Cleutjens KBJM, Kessels AGH, Kitsllar PJEHM, Borgers M, Frederik PM, Daemen MJPM, Engelshoven JMAV. Accumulation of Ultrasmall Superparamagnetic Particles of Iron Oxide in Human Atherosclerotic Plaques Can Be Detected by In Vivo Magnetic Resonance Imaging. Circulation. 2003; 107(19):2453–2458. [PubMed: 12719280]
76. Choi HS, Liu W, Misra P, Tanaka E, Zimmer JP, Ipe BI, Bawendi MG, Frangioni JV. Renal clearance of quantum dots. Nature Biotechnology. 2007; 25(10):1165–1170.
77. Jiang W, Kim BYS, Rutka JT, Chan WCW. Nanoparticle-mediated cellular response is size-dependent. Nature Nanotechnology. 2008; 3(3):145–150.

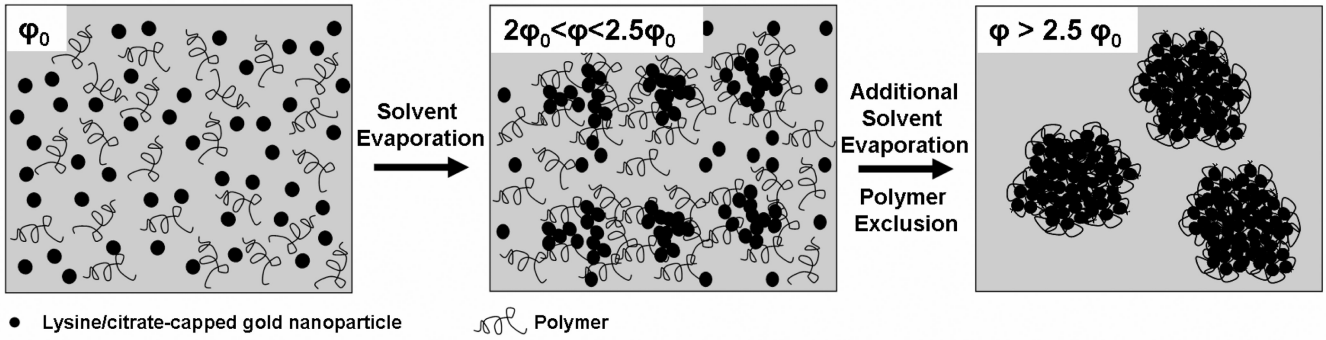

Figure 1.

Schematic of kinetically controlled assembly process of nanocluster formation, in which primary gold nanoparticles aggregate in the presence of a weakly adsorbing polymer, PLA-*b*-PEG-*b*-PLA micelles, in a controlled manner to yield sub-100 nm clusters. Weak polymer adsorption increases counter ion binding and reduces the surface charge on the gold nanoparticles to facilitate cluster nucleation. Cluster growth is facilitated by increasing the volume fraction of particles, ϕ, via solvent evaporation. PEG blocks on the polymer extend into the aqueous environment and provide steric stabilization to clusters.

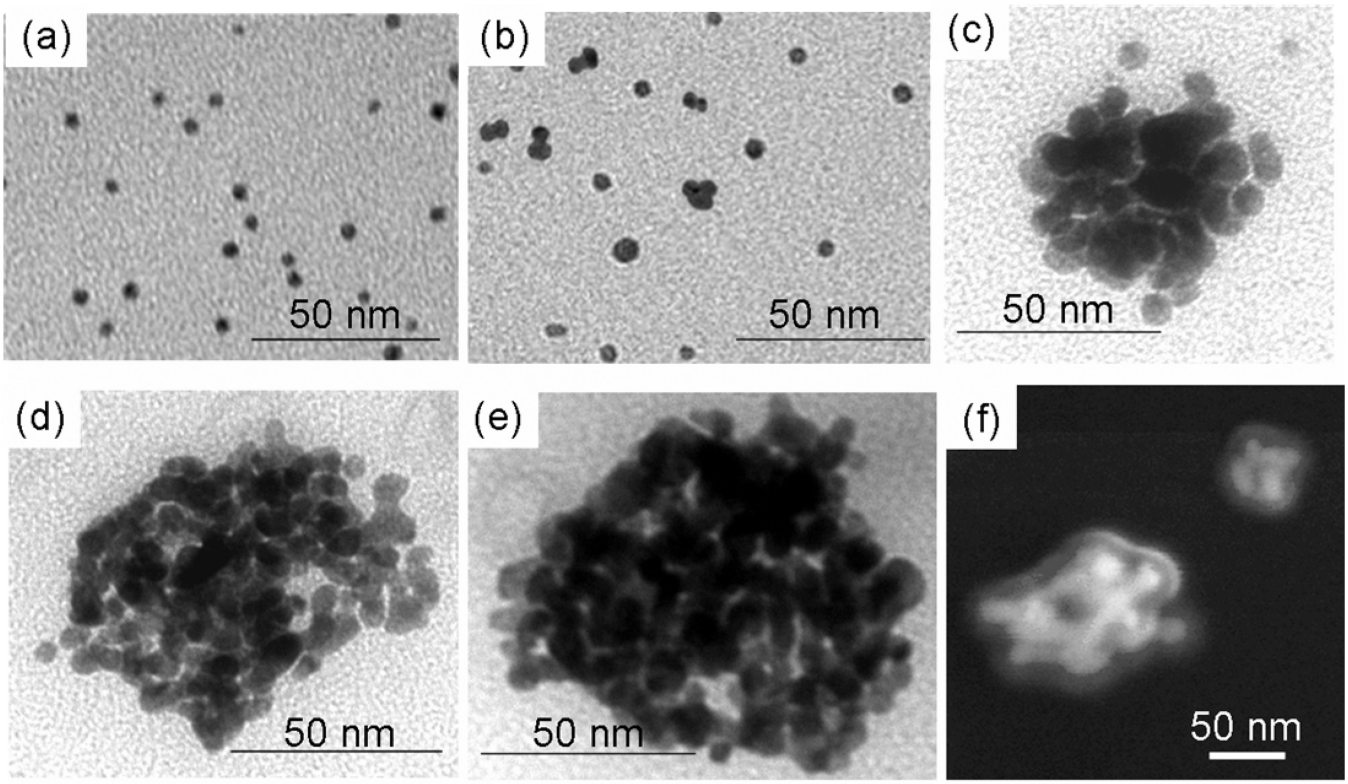

Figure 2.
TEM images of nanoclusters produced after (a) 0%, (b) 50%, (c) 60%, (d) 80%, (e) 100% solvent evaporation. (f) SEM image of nanoclusters produced after 100% solvent evaporation. The nanoclusters were formed at an initial gold concentration of 3 mg/mL and a PLA-*b*-PEG-*b*-PLA concentration of 50 mg/mL.

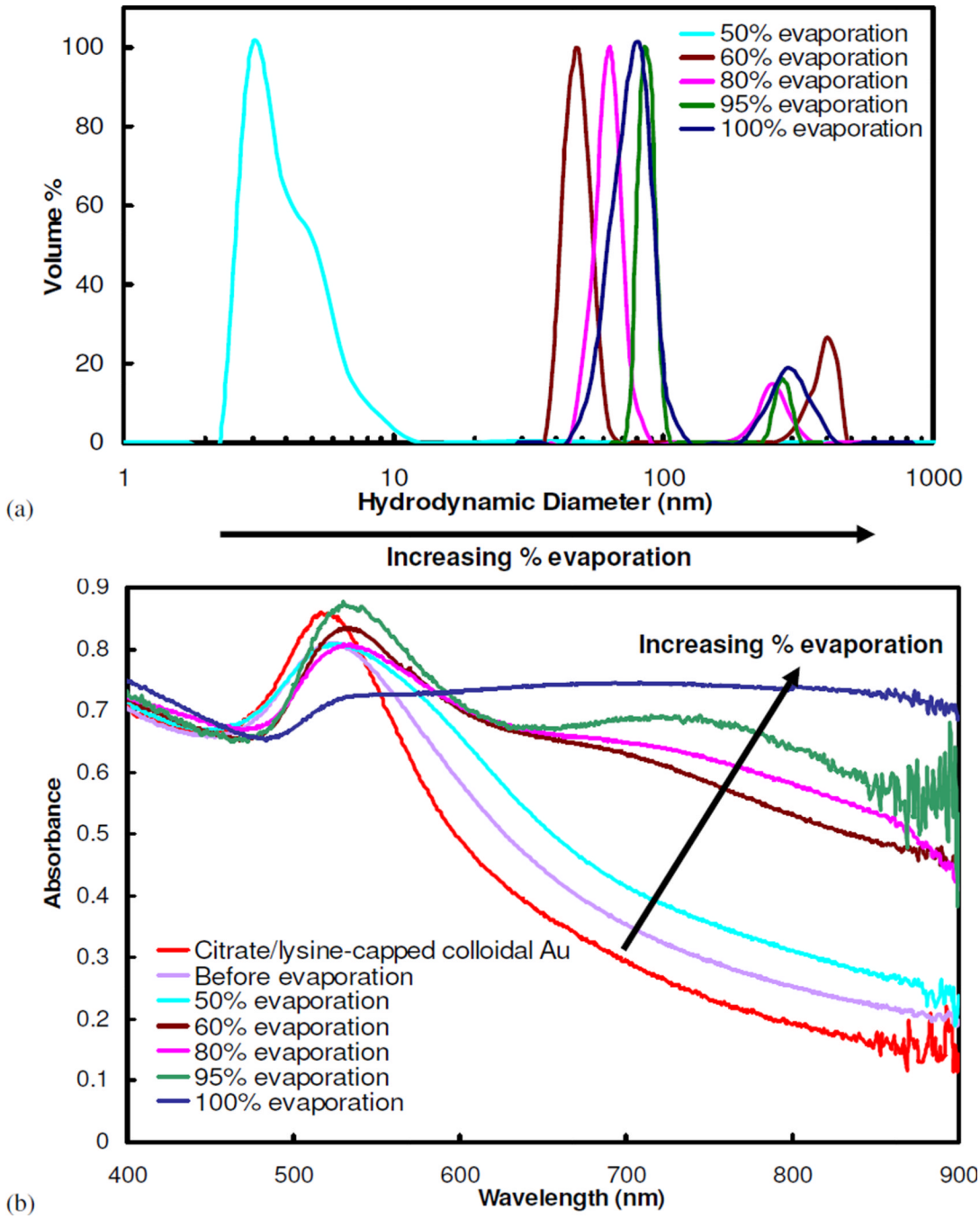

Figure 3.

(a) Particle size measurements, by DLS, and (b) UV-vis absorbance spectra for nanoclusters composed of citrate/lysine-capped gold nanoparticles produced after different extents of evaporation. Nanoclusters were produced at a starting gold concentration of 3 mg/mL and bound together with PLA-*b*-PEG-*b*-PLA at a polymer/gold ratio of 16/1.

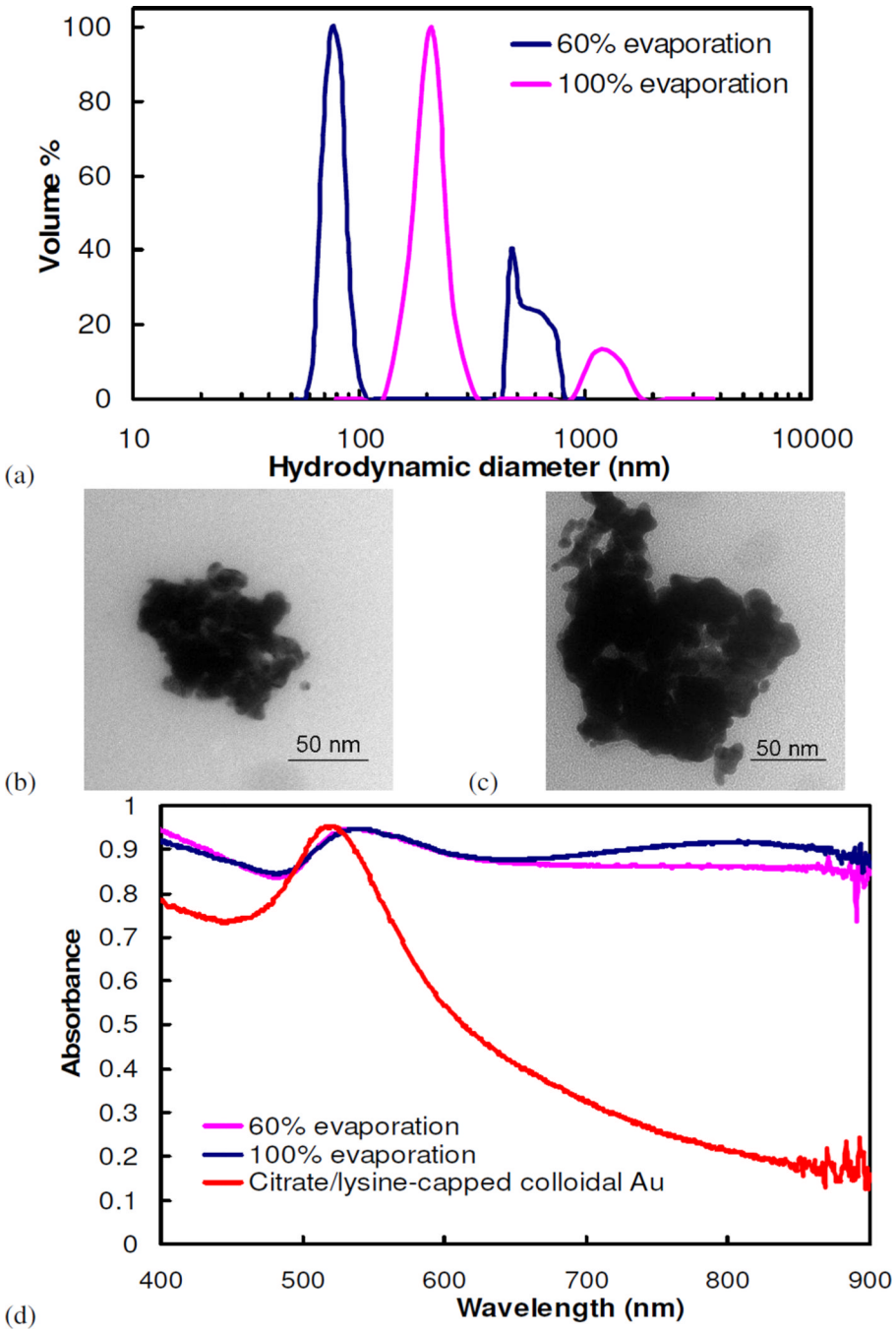

Figure 4.

(a) Particle size measurements, by DLS, TEM images of nanoclusters after (b) 60% and (c) 100% solvent evaporation, and (d) UV-vis absorbance spectra of nanoclusters composed of citrate/lysine-capped nanoparticles assembled using PEG homopolymer (MW=3350). The starting gold and polymer concentrations were 3 mg/mL and 50 mg/mL, respectively.

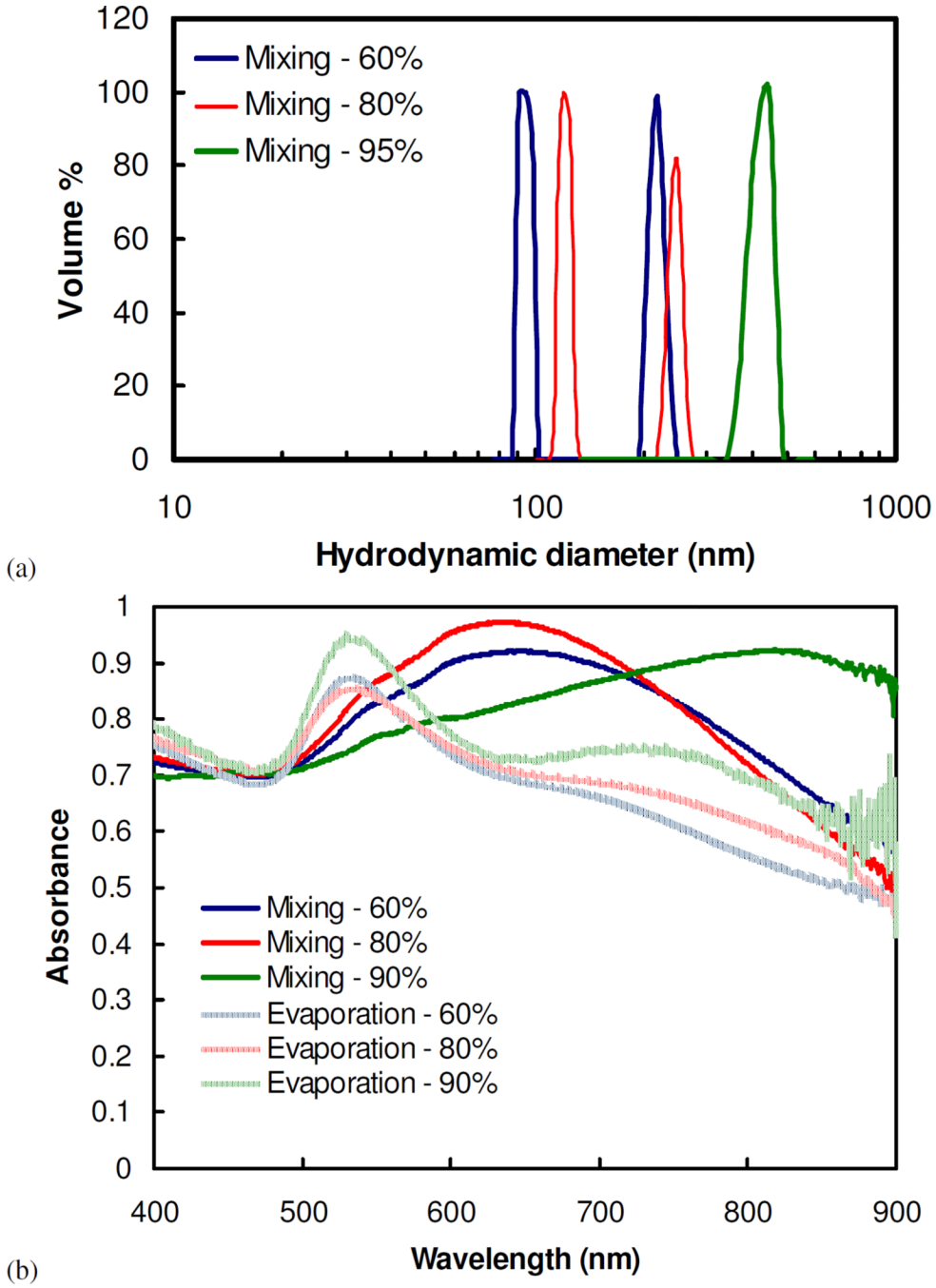

Figure 5.

(a) Particle size distribution, as measured by DLS, and (b) UV-vis spectra of clusters of citrate/lysine-capped nanoparticles made with the mixing protocol. The conditions of cluster formation are equivalent to that for clusters formed by solvent evaporation at a starting gold concentration of 3 mg/mL and a PLA-*b*-PEG-*b*-PLA/Au ratio of 16/1. In (b), the UV-vis spectra are compared to that for nanoclusters produced using solvent evaporation.

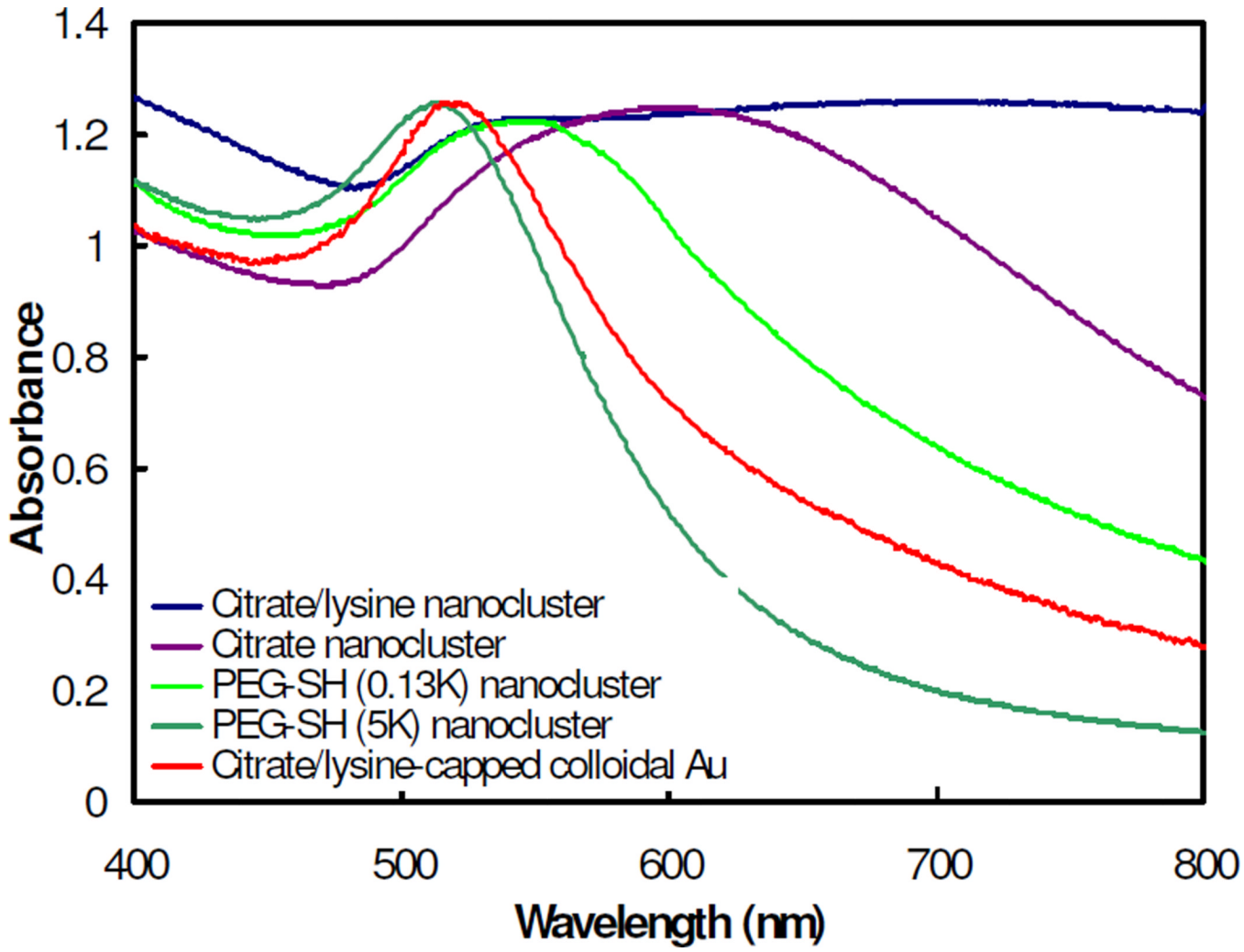

Figure 6.
UV-vis absorbance spectra for clusters made with gold primary particles capped with different ligands. The clusters were produced using a starting gold concentration of 3 mg/mL and bound together using PLA-*b*-PEG-*b*-PLA at a 16/1 polymer/Au ratio. The clusters were formed under 100% solvent evaporation.

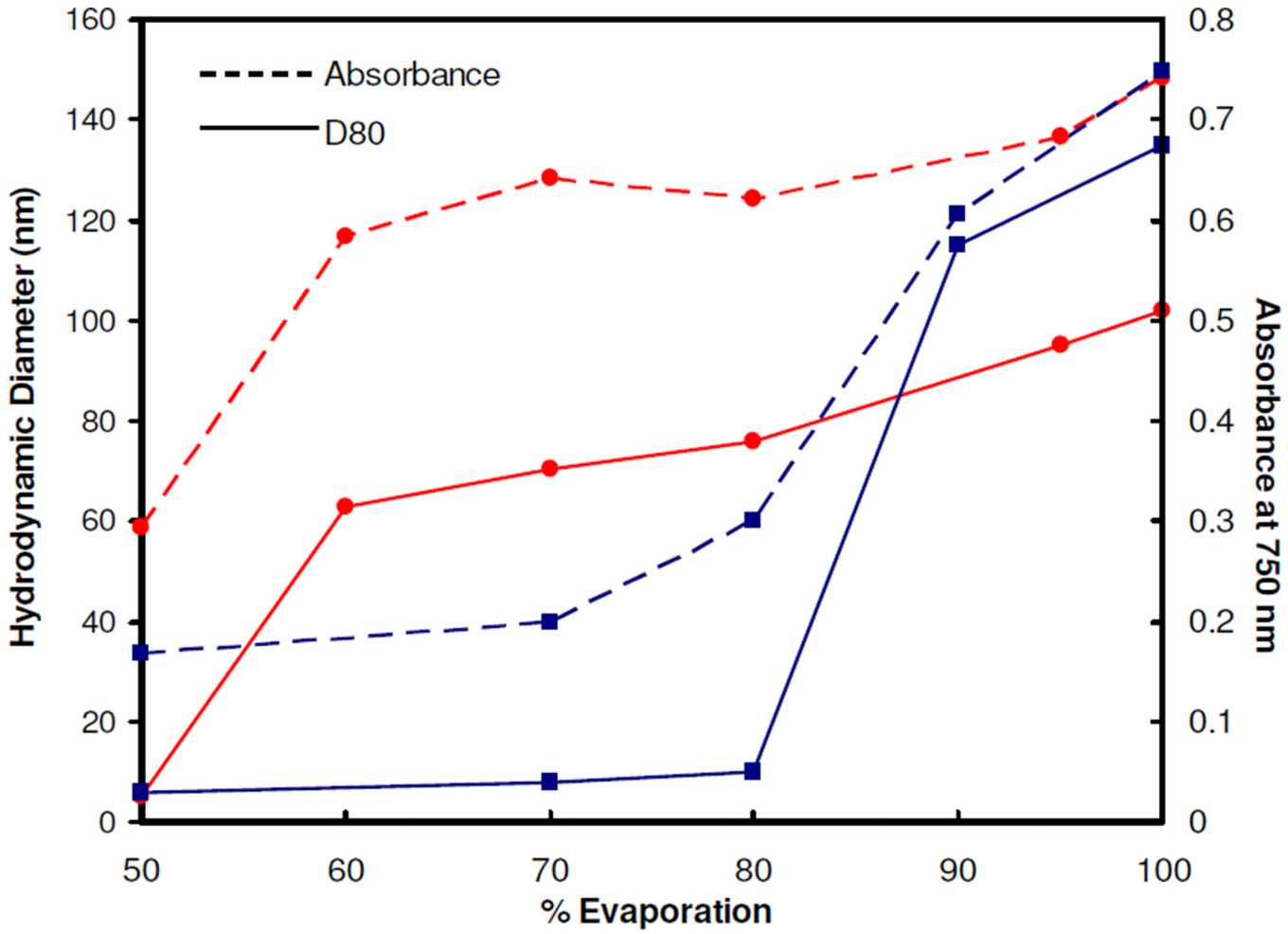

Figure 7.

Hydrodynamic diameter (D80) and absorbance values for nanoclusters composed of primary particles capped with citrate (■) or a combination of citrate and lysine (●) ligands. The clusters were produced using a starting gold concentration of 3 mg/mL and bound together using PLA-*b*-PEG-*b*-PLA at a 16/1 polymer/Au ratio.

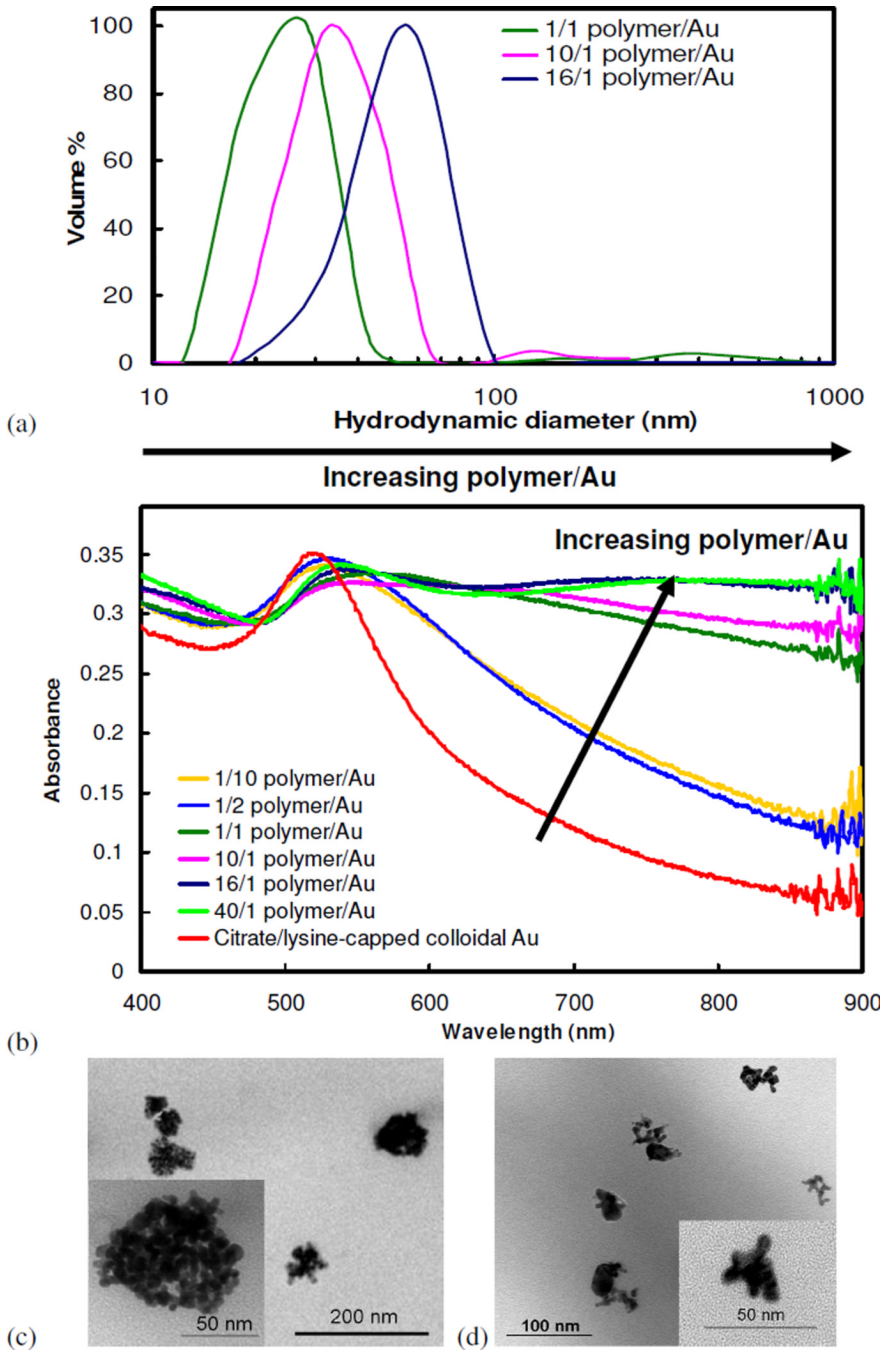

Figure 8.

(a) Particle size distribution, as measured by DLS, and (b) UV-vis absorbance spectra of nanoclusters of citrate/lysine-capped nanoparticles produced with varying PLA-*b*-PEG-*b*-PLA/gold ratios at an initial gold concentration of 1 mg/mL and 100% solvent evaporation. TEM images of nanoclusters: (c) 16/1 polymer/gold ratio and an initial gold concentration of 3 mg/mL and (d) a 1/1 polymer/gold ratio with an initial gold concentration of 1 mg/mL after 100% solvent evaporation.

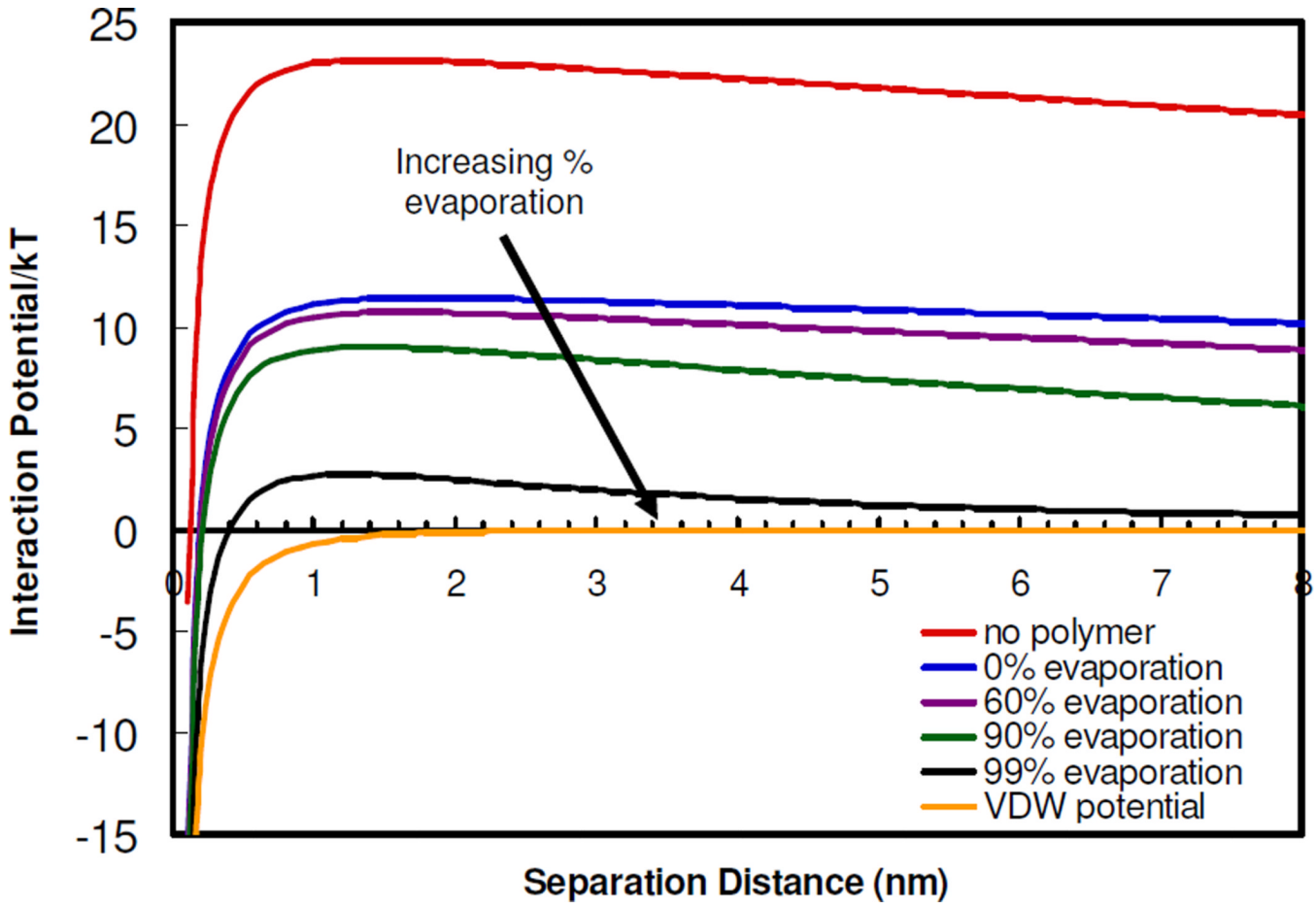

Figure 9.

Van der Waals and total interaction potentials describing the stability of citrate/lysine-capped gold nanoparticles in the absence of PLA-*b*-PEG-*b*-PLA and after the addition of PLA-*b*-PEG-*b*-PLA. Effects of solvent evaporation on the total interaction potentials are shown.

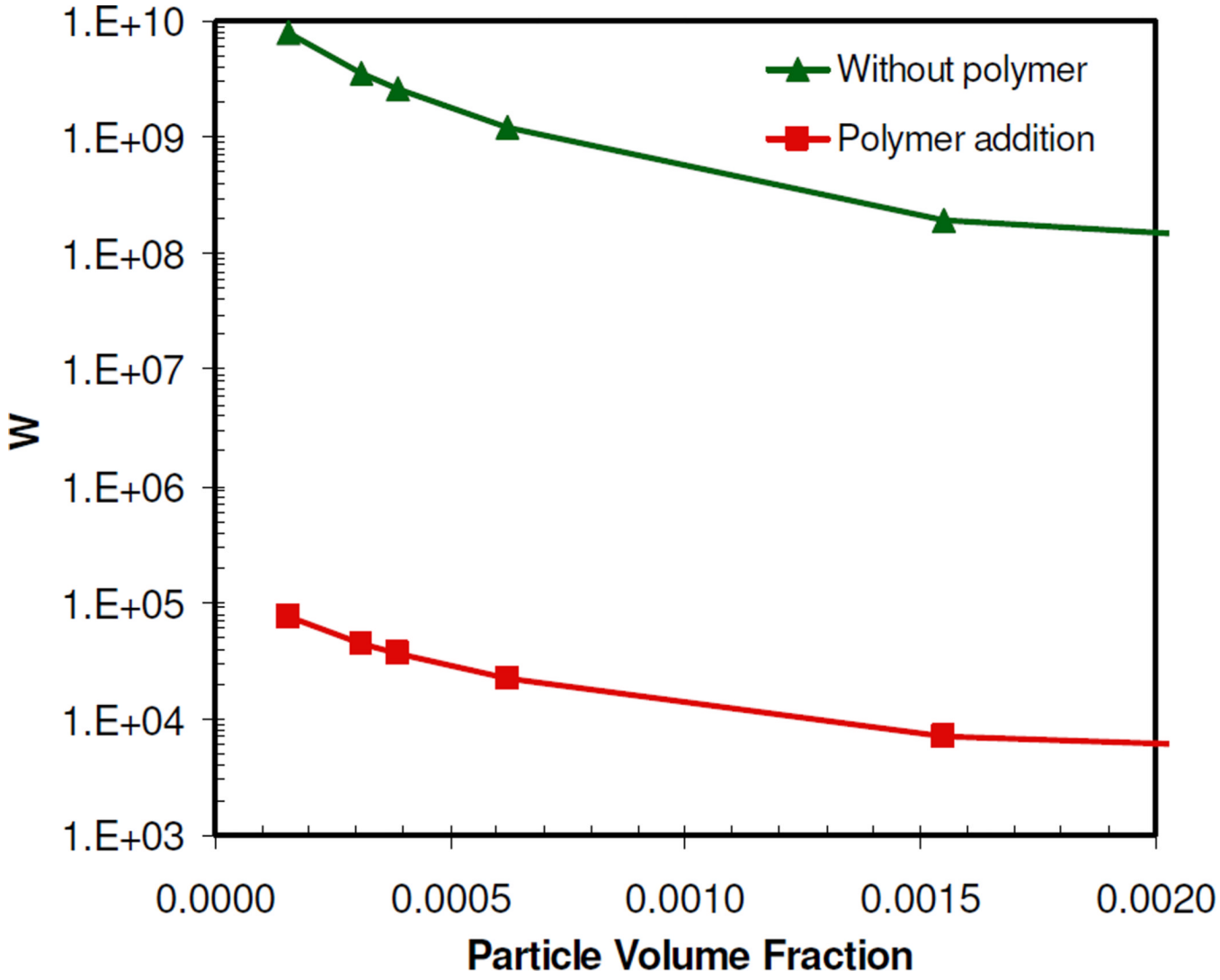

Figure 10.
Stability ratio of a system of citrate/lysine-capped gold nanoparticles in the absence and presence of PLA-*b*-PEG-*b*-PLA determined using DLVO theory, as a function of particle volume fraction.

Table 1

Zeta potentials of gold primary particles and nanoclusters capped with citrate or a combination of citrate and lysine ligands.

Ligand	Zeta potential (mV)
Citrate (primary particle)	−44.0 ± 4.9
Citrate/lysine (primary particle)	−30.1 ± 2.4
PLA(2K)-*b*-PEG(10K)-*b*-PLA(2K)	−8.0 ± 0.2
Citrate/lysine 16/1 PLA-*b*-PEG-*b*-PLA/Au (nanocluster – 100% evaporation)	−16.3 ± 4.0
Citrate 16/1 PLA-*b*-PEG-*b*-PLA/Au (nanocluster – 100% evaporation)	−13.0 ± 3.3

Table 2

Calculated stability ratios for nanoclusters produced using citrate/lysine-capped nanoparticles at a 16/1 PLA-*b*-PEG-*b*-PLA /Au ratio and a starting gold concentration of 3 mg/mL.

Evaporation Extent (%)	N_0 (particles/m^3)	$t_{1/2,f}$ (s)	t_{col} (s)	$t_{1/2,s}$ (s)	W
0, no polymer	5×10^{21}	3.93×10^{-5}	2.59×10^{6}	256634	6.60×10^{9}
0, polymer	5×10^{21}	1.51×10^{-4}	3.60×10^{3}	356	3.97×10^{5}
50	1×10^{22}	1.30×10^{-4}	300	30	2.50×10^{5}

Table 3

Size distribution moments and cluster yields, as determined by FAAS, for nanoclusters produced using different extents of evaporation. The initial gold concentration was 3 mg/mL and the PLA-*b*-PEG-*b*-PLA / gold ratio was 16/1.

Sample	Cluster yield (%)	μ_1	μ_3
Citrate/lysine-capped nanoclusters 100% evaporation	99.7	1.11	0.93
Citrate/lysine-capped nanoclusters 80% evaporation	96.8	1.04	0.97
Citrate/lysine-capped nanoclusters 60% evaporation	95.1	1.09	0.93
Citrate-capped nanoclusters 100% evaporation	98.5	1.01	0.99